F-111C Lower Wing Skin Bonded Composite Repair Substantiation Testing

R. Boykett and K. Walker

DEPARTMENT OF DEFENCE
DEFENCE SCIENCE AND TECHNOLOGY ORGANISATION

F-111C Lower Wing Skin Bonded Composite Repair Substatiation Testing

R. Boykett and K. Walker

Airframes and Engines Division
Aeronautical and Maritime Research Laboratory

DSTO-TR-0480

ABSTRACT

Experimental testing was undertaken to verify a bonded composite repair to a crack in the primary structure of a F-111C aircraft of the Royal Australian Air Force. The flight safety was compromised by a crack in the lower wing skin reducing the structure residual strength below the Design Limit level. Two levels of representative specimens were designed to incorporate the complex local geometry in the lower wing skin. They were tested in several configurations (ambient, high and low temperature) under static and cyclic loads with, and without, repaired cracks. Extensive strain survey data was obtained for both types of specimens and their static residual strength was shown to be restored by the repair. Cyclic loading tests of specimens with the repair also demonstrated good durability and damage tolerance, with crack growth data providing a recommended inspection interval for remaining aircraft.

RELEASE LIMITATION

Approved for public release

DEPARTMENT OF DEFENCE

DEFENCE SCIENCE AND TECHNOLOGY ORGANISATION

Published by

DSTO Aeronautical and Maritime Research Laboratory
PO Box 4331
Melbourne Victoria 3001

Telephone: (03) 9626 7000
Fax: (03) 9626 7999

AR-010-110
November 1996

APPROVED FOR PUBLIC RELEASE

F-111C Lower Wing Skin Bonded Composite Repair Substatiation Testing

Executive Summary

This report documents the results of a comprehensive testing program for the substantiation of a bonded boron epoxy patch repair to a fatigue crack in the lower wing skin of an F-111C aircraft (A8-145) in the Royal Australian Air Force. The fatigue crack was a chordwise 48 mm crack in the critical, non-failsafe, port lower wing skin at approximately 2/3 semi span. The crack had reduced the wing's residual strength to below Design Limit Load and the repair was therefore critical; the options were to scrap the whole wing or apply a bonded repair. This repair represents the most critical application of bonded repair technology yet undertaken anywhere in the world.

As this is the first time that a bonded composite repair has been applied to critical damage in primary aircraft structure, the repair substantiation requirements were particularly stringent. The Aeronautical and Maritime Research Laboratory was to provide an independent stress analysis (Finite Element Method) and a testing program of representative specimens.

Static and fatigue tests were carried out on two levels of representative specimens; simple panel specimens and more complex, quasi-full-scale, box specimens. The tests showed that the repair restored the static strength of the specimens far above Design Limit. Although crack growth was not halted by the repair in fatigue tests, it was reduced significantly to allow convenient inspection intervals, thus demonstrating that it has adequate durability and damage tolerance characteristics. The results give confidence in the original design and application procedures which were in accordance with RAAF Engineering Standard C5033.

This work has set a precedent for providing an effective and efficient substantiation for such critical repairs to primary structure. The work also represents a significant step in the transfer of technology from the Defence Science and Technology Organisation to the RAAF.

Authors

R. Boykett
Airframes and Engines Division

Robert Boykett is a graduate of the Royal Melbourne Institute of Technology with a Bachelor Degree of Engineering (Aeronautical) in 1984. At the Government Aircraft Factories, 1985 - 1990, (now Aerospace Technologies of Australia) he undertook detail design and stress analysis of civil and military aircraft components in production, including repairs to metallic and composite structures. His work at the Aeronautical and Maritime Research Laboratory, since 1990, has been in the field of structural testing, including the development of the full-scale fatigue test rig for the F/A-18 International Follow-On Test Project. He is currently responsible for a validation test program on a bonded composite repair.

K. Walker
Airframes and Engines Division

Kevin Walker graduated in 1983 with a Bachelor of Aeronautical Engineering (with distinction) from RMIT. He then served for eight years with the RAAF, including a posting to the USA where he gained a Masters of Science in Aeronautics and Astronautics from Purdue University. He then worked for three years in private industry before joining AMRL in early 1994. His work at AMRL included fatigue and damage tolerance analysis studies and aircraft load spectrum determination using the Aircraft Fatigue Data Analysis System (AFDAS). He is currently also task manager "Analysis and Validation of Design Procedures for Bonded Repairs".

Contents

List of Abbreviations

AFDAS	Aircraft Fatigue Data Acquisition System
AMRL	Aeronautical and Maritime Research Laboratories
CPLT	Cold Proof Load Test
DADTA	Durability And Damage Tolerance Analysis
DLL	Design Limit Load
DSTO	Defence Science and Technology Organisation
DUL	Design Ultimate Load = DLL x 1.5
EDM	Electro Discharge Machining
F-111C	General Dynamics aircraft used by RAAF
F-111G	General Dynamics aircraft used by USAF
FALSTAFF	Fighter Aircraft Loading Standard for Fatigue evaluation
FASS	Forward Auxiliary Spar Station
FEM	Finite Element Modelling/Methods
GD	General Dynamics (who designed and built F-111 aircraft)
Lockheed	Lockheed Martin is the company that owns GD
NDI	Non Destructive Inspection
RAAF	Royal Australian Air Force
USAF	United States Air Force

1. Introduction

A crack was discovered in the port lower wing skin of a Royal Australian Air Force F-111C aircraft (RAAF tail number A8-145) during a routine visual inspection. The initial indication was fuel seepage at the site of an apparent 40 mm chordwise crack; however, a detailed non-destructive inspection revealed a through-thickness crack, 48 mm long tip-to-tip. Fracture mechanics calculations indicated that the residual strength had been degraded to 150 MPa (21.7 ksi), which is considerably less than the Design Limit Stress of 256 MPa (37.1 ksi) specified for this region of the wing[1], compromising flight safety.

A mechanically fastened metallic doubler repair option was rejected for a range of reasons, including undesirable aerodynamic implications and because the underlying structure could not be inspected. The only viable alternative to scrapping the wing was a bonded repair. A bonded boron fibre epoxy repair was designed and implemented by RAAF personnel, on the basis of design principles and application procedures developed by DSTO,[2,3] now incorporated by the RAAF into an Engineering Standard (C5033)[4]. Because the repair is to primary structure, comprehensive substantiation is needed to certify its airworthiness; Aeronautical and Maritime Research Laboratory (AMRL) is responsible for an independent validation of the repair design through Finite Element Modelling (FEM) and substantiation of the repair through representative specimen testing.

A statement of requirements[5], defines the substantiation testing to be carried out by AMRL. Details are as follows :

- Verify that the residual strength after repair is acceptable;
- Verify that the residual strength degradation in-service after the repair is acceptable;
- Verify that the load spectrum developed for this location is reasonably representative;
- Quantify thermal effects due to the patch application procedure;
- Quantify the environmental degradation effects.

A crack was found in the same location in a United States Air Force (USAF) F-111G wing 40 mm long. This section of the skin was cut out and one of the fracture surfaces provided to AMRL to assist with the repair analysis. It is referred to as "the USAF specimen" in this report.

Figure 1 indicates the location of cracking on the lower wing-skin. Raised portions serve as integral stiffeners and as attachment lands for spars. The cracking occurred in an area lying below the forward auxiliary spar, at the spar station FASS 281.28, where the thickness of the integral stiffener is reduced from approximately 8.2 mm to the nominal skin thickness (3.7 ± 0.1 mm at this location). The purpose of this depression in the stiffener is to allow full fuel flow and drainage between adjacent bays of the

wing-box fuel tank. Two side-stiffeners compensate for the loss of spanwise stiffness due to this fuel-flow passage, as indicated in Fig. 1. The thickness variation in this region is more clearly illustrated in Figure 2. This asymmetrical geometry leads to a significant stress concentration factor and to out-of-plane secondary bending at the location where cracking occurs[6].

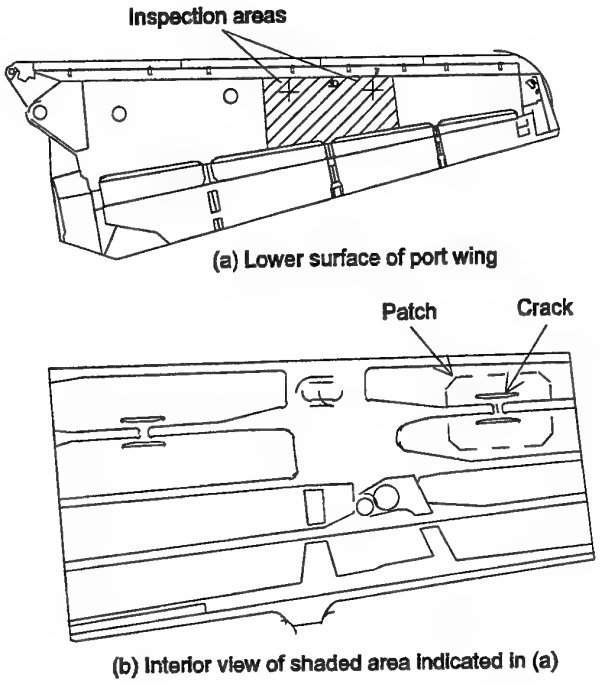

Figure 1. Crack location on the F-111C lower wing-skin and repair patch outline.

The cracking occurs in the chordwise direction, normal to the direction of the nominal principal stress from wing bending at that location. The presence of secondary bending loads results in the crack initially growing from the inside surface towards the outside surface with faster crack growth along the wing-skin's inner surface relative to its outer surface. This effect is clearly visible in the USAF specimen (refer to section 6). The discrepancy between the surface traces is further accentuated by the residual compressive stress at the outer surface caused by shot peening. For the purposes of assessing the residual strength, however, it is convenient to assume a straight-fronted through-crack, as indicated by the shaded area in Figure 2. This leads to the residual strength estimate of 150 Mpa.

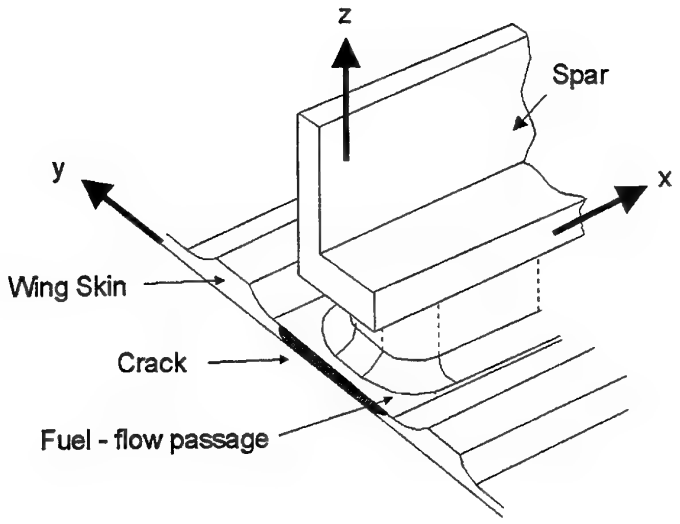

Figure 2: Local geometry of the lower wing skin in the vicinity of the fuel-flow passage, showing the location of cracking and the coordinate axes used in the text.

2. Test article plan

2.1 Specimens

A range of tests were undertaken on twenty panel specimens, two box specimens and six coupon specimens to fulfil the requirements noted in section 1, above. Several specimens had more than one test performed on them ; a list of specimen configurations, load conditions and test result summary is shown in Appendix 1.

The simple panel specimens were only representative of the aircraft lower wing skin and were used for most tests to determine static and fatigue strength. The two complex box specimens were representative of the aircraft lower wing skin and spars; these were used to validate the tests on the panel specimens.

Six coupon specimens were to tested to obtain values of the fracture toughness (K_c) for comparison with values used in the RAAF analysis with C5033. These were uniaxial static tests to failure of precracked coupons representative of the wing skin material and nominal thickness.

2.2 Test equipment

Since the loading of this part of the aircraft wing skin is considered to be dominated by the wing bending loads, the loads applied to all specimens are uni-axial tension and

compression. Servo-hydraulic testing machines of the appropriate load capacity for static and dynamic loading are available in the Wills Fatigue Laboratory (AMRL - Fishermens Bend). Tests were carried out over an eighteen month period, unless noted, under ambient laboratory conditions - typically between 20° and 25°C. Some panel specimens were tested at hot (+110°C) or cold (-40°C) temperature extremes by enclosing them in an environmentally conditioned chamber ; humidity was not controlled. Some elevated temperature tests were done using infra-red lamps to heat panel specimens to 80°C.

2.3 Test loading

Loads are derived from the multi-channel recorder data (from the RAAF fleet) in terms of the bending moment at the wing root pivot, and corrected for the spanwise location using the aircraft manufacturer's design load distribution. The Design Limit Stress for this area is thus 256 MPa.[21] The Design Limit Load (DLL) for each specimen is calculated to be the Design Limit Stress multiplied by the cross-sectional area of the central test section, ignoring the effects of crack size and the boron repair patch. The area of the webs in the box specimen is included but the bending restraint on the panel specimen is not considered effective in carrying axial load.

2.3.1 Static tests

Tensile tests to failure were undertaken at a slow ramp rate (1 kN per second) on panel specimens in different configurations (pre-cracked or not, patched or not) under a variety of conditions (at ambient temperature, -40°C, +110°C). See Appendix 1.

2.3.2 Fatigue tests

The fatigue load spectrum originates from that used in the RAAF F-111C Durability and Damage Tolerance Analysis (DADTA) performed by Lockheed. The spectrum is representative of the fleet and consists of a block representing 200 flights (500 hours of flying).[13] The test spectrum loading consists of two parts, the first being the flight load spectrum described above, and the second being the Cold Proof Load Test (CPLT). The RAAF fleet has the CPLT applied to each F-111C every 2000 flight hours in a special USAF facility in Sacremento (U.S.A.) that can test the structure whilst conditioned to -40°C. The CPLT case starts and finishes at zero and consists of four static load turning points, each representing a flight manoeuvre as shown below. The panel specimens were originally designed to be loaded only in tension but their lack of stability in compression led to test loads being clipped to -50 kN maximum.

Turning point	1st	2nd	3rd	4th
G-level	-2.4	+7.33	-3.0	+7.33
Equivalent load (kN)	-77.8	+193.8	-96.0	+193.8
Test load (kN)	-50	+193.8	-50	+193.8

Figure 3. Cold Proof Load Test values for panel specimens

The values for box specimens are proportional to cross-sectional area.
Three fatigue spectrums have been used in these tests ; unless specified, the testing (including CPLT) was at ambient temperature:

- A simple, severe constant amplitude spectrum, ranging from zero to 80% DLL (tension) was applied to one panel specimen to get an indication of durability under the most abusive stress conditions.

  The next fatigue spectrum was blocked into nine ranges and truncated to reduce the number of turning points in the DADTA spectrum from approximately 1.5 million to 8,628 turning points (ranging from -50 kN to +177.2 kN on the panels). This load block representing 100 flight hours is shown below in Figure 4. The spectrum was then clipped at -8.75 ksi due to stability limitations of the panel specimen under compression loading.

Exceed-ences	**Total occurrences**	**Min Stress (ksi)**	**Max Stress (ksi)**	**Min stress (MPa)**	**Max stress (MPa)**
2	2	-12.300	31.000	-84.809	213.745
8	6	-8.957	29.362	-61.757	202.451
21	13	-6.575	27.725	-45.333	191.164
43	22	-5.032	26.088	-34.695	179.877
113	70	-3.489	24.45	-24.056	168.583
470	357	-1.727	22.813	-11.907	157.296
1344	874	0.055	21.175	0.379	146.002
2053	709	0.331	19.538	2.282	134.7151
8628	6575	0.607	17.900	4.185	123.417

Figure 4. Blocked load spectrum

- The final fatigue spectrum truncated the DADTA spectrum on the basis of constant amplitude crack propagation results[33], and used a discriminant of 5 ksi to give a cycle-by-cycle spectrum of 36,273 turning points for a load block representing 500 flight hours.[13] This spectrum is less severe than the first blocked spectrum and is also considered less severe than the standard FALSTAFF spectrum. It was also clipped at -8.75 ksi to meet the requirement for a maximum compression load of -50 kN in the panel specimens and, for consistency, -352 kN in the box specimens.

2.3.3 Strain surveys

Several specimens were fitted with an array of electrical resistance strain gauges; axial surface strains could be determined from voltages recorded at each static load level.

Two panel specimens were tested in this manner with no crack damage or repair applied. Two other panel specimens were tested with a pre-crack and repair patch applied so that the thermal strains induced by (i) the adhesive cure and (ii) the elevated temperature environment could be investigated[24].

The first box specimen strain survey investigated the strain distribution in the unpatched, uncracked condition so that a comparison could be made with results from the smaller panel specimens [7,8], the Finite Element models [5,9] developed at AMRL and the full-scale wing test[10]. The second box specimen had 34 strain gauges fitted to one of the boron patches so that the thermal strains induced by the adhesive cure could be investigated[17].

2.3.4 Crack Initiation

Most test specimens had a flaw introduced mechanically in the area where cracking initiated in the aircraft. Three panel specimens (with no flaw) were used to investigate the initiation of cracking under the cycle-by-cycle spectrum until the crack grew to the size of the USAF specimen (40 mm) . These tests verify the representative nature of the panel specimen design and aid in the analysis of inspection intervals for the remaining F-111C that do not have the repair in the RAAF fleet.

2.3.5 Temperature and Frequency Effects

Two panel specimens were prepared with damage (40 mm pre-crack) and the patch repair, before being tested under the cycle-by-cycle spectrum to verify the crack growth rate. Four test configurations were at ambient (23°C) and 80°C (the cure temperature of the repair adhesive) at loading frequencies of 5.0 and 0.5 Hertz.

3. Panel specimen testing

3.1 Panel specimen description

Skin panel specimens contain a test section that is a full-scale replica of the F-111C aircraft's fuel flow passage in the lower wing skin at FASS 281.28.

The specimen material is Aluminium 2024 - T851 and is machined to final size. It is hand finished in some areas by polishing and peening to aid crack measurement, and to prevent failure outside the test area of the specimen.

The panel specimen design was later modified to allow compression loads to be safely applied. It could have a bending restraint attached to minimise the amount of out-of-plane deflection when the asymmetric cross-section is loaded. Slotted holes in the bending restraint and teflon washers prevent it acting as an axial doubler.

The introduction of the crack defect into the specimens was achieved by creating a notch in centre of the side representing the inner surface of the lower wing skin using Electro Discharge Machining (EDM). The specimen was then loaded under constant amplitude cyclic tension until a crack appeared at each end of the notch and grew to the required length. This crack defect was similar in size and shape (40 mm through-thickness crack) to that in the specimen supplied from the USAF F-111G wing.

Patching was done (after pre-cracking) to the specimen side representing the outer surface of the lower wing skin after it was carefully cleaned, grit blasted and treated with an adhesion promoter to ensure a good bond surface. Repair patches were made from Boron/Epoxy pre-preg fibre composite 5521-4.[11] The patch designed for the panel was not as long (reduced overlap) or wide (no taper), and was, therefore, a conservative version of that carried out for the repair on RAAF aircraft A8-145.[12] The pre-cured patch was bonded using FM-73 adhesive cured at 80° Celsius. Finally, non destructive inspection (NDI) of the patched area confirmed patch and bond integrity.

Details of the panel specimen, including strain gauge locations, are in Appendices 2 and 3.

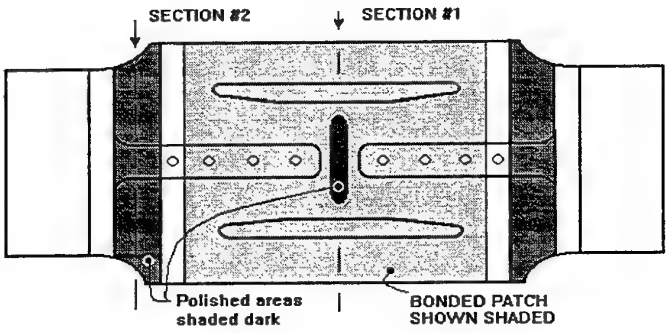

Figure 5. Panel specimen.
View onto side representing upper surface of lower wing skin.
Boron \ Epoxy patch is bonded to side representing lower surface.

3.2 Static strength results

Static residual strength tests were undertaken by loading specimens in uni-axial tension until failure occurred. All specimens broke in two pieces at failure.[14]

The results of five static tests on five panel specimens are summarised in Figure 6 below. The residual strength (stress MPa) is calculated from the failure load and the nominal cross-sectional area (829 mm^2 , ignoring the patch and crack).

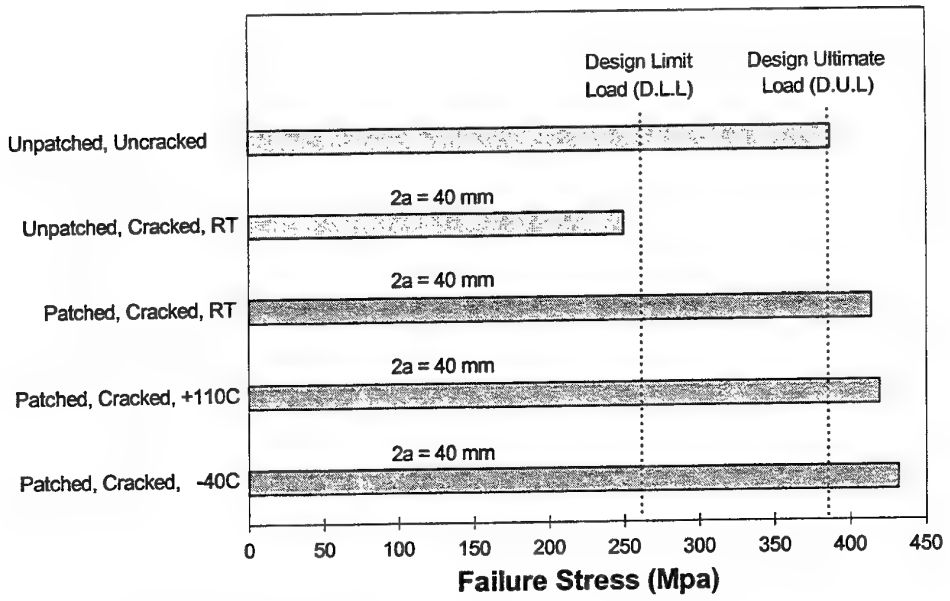

Figure 6. Results of static strength tests on panel specimens.

Note:

1) The undamaged "baseline" panel fails at DUL but the unrepaired damaged panel does not meet DLL. This was predicted by fracture mechanics calculations[1].

2) The repaired panels all exceed DUL, with little effect noted between the different temperatures. The temperature gradient on the specimen during the hot test (+110°C) ranged from 83.0°C to 119.4°C, and during the cold test (-40°C) from -16.3°C to -42.2°C. The maximum values were at the centre of the specimen due to heat transfer from the ends of the specimen into the grips of the testing machine[14]. However, the hot test was repeated at later date (August 1996) using a new environmental chamber. The specimen *FLTP-17* had already been used for fatigue loading (50,000 simulated flight hours and the crack had grown to 69.4 mm). The temperature range on the specimen was 105°C to 112°C, within the boundary of the boron patch, when it failed by the crack propagating to the edges at a load of 204.7 kN (247 Mpa). Since the Design Ultimate Stress for the high temperature load case[7] is 214.5 Mpa, the specimen *FLTP-17* demonstrated that the repair restores static strength above DUL at high temperature. This is considered to be a remarkable achievement for the FM73 adhesive because 110°C is well above the glass transition temperature, T_G

3) The "baseline" specimen and the first hot test specimen both failed outside the test section.

3.3 Strain survey results

3.3.1 Undamaged panel specimens

Strain survey tests were undertaken on two uncracked, unpatched panel specimens[7,8]. The first test used a specimen without a bending restraint and highlighted unexpected non-linear behaviour. The strain gauge layout included positions also used in strain survey tests of a full size F-111A wing at AMRL[10], and of the first box specimen[17]. A comparison of the strain survey results from all three is given in section 4.2.

Tests on the second specimen recorded data from load runs with and without the bending restraint attached. The bending restraint uses fasteners pitched as per the aircraft spar (initially, four fasteners each side of the fuel flow recess in the centre of the specimen) and results showed that the restraint significantly influences the strains in the central area. Refer to Figure 7, below, for results, and Figure 27 (Appendix 2) for details of strain gauge locations. Further tests showed that reducing the number of fasteners from four to three made no change to the strain distribution.

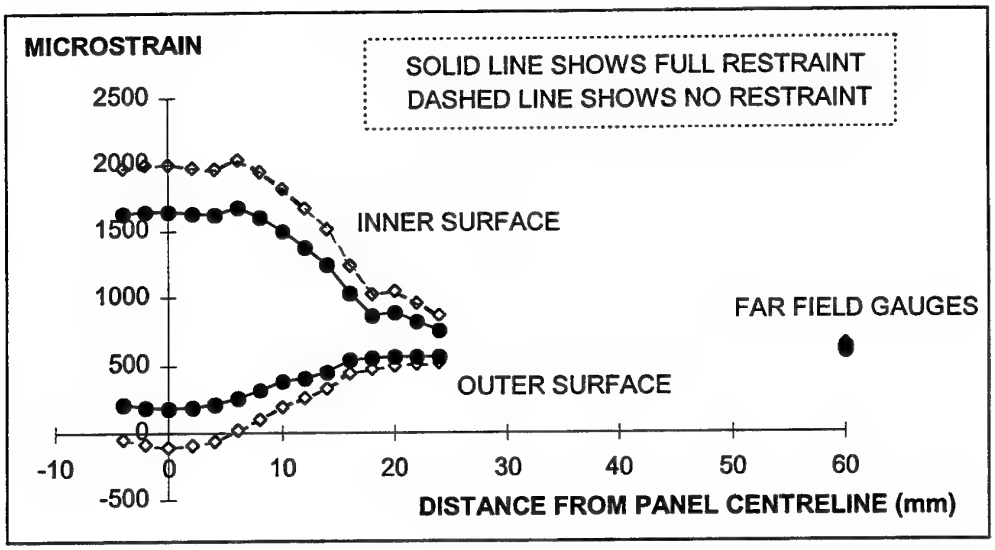

Figure 7. Chordwise strain distribution at 20% DLL (after CPLT case)

Note that the high strain variation reduces to within 25% of the nominal (far-field) value within 20 mm of the panel centreline (representing the spanwise spar line). The crack in RAAF aircraft A8-145 was 48 mm tip-to-tip (symmetrical about the spar line).

Note also that the peak strain on the inner surface at 20% DLL is approximately 1600 microstrain. Assuming a linear relationship with loading, this equates to approximately 8000 microstrain at 100% DLL , which is well in excess of the uni-axial yield strain for the material of 5500 microstrain. Even allowing for some degree of non-linearity, this result indicates that significant yielding can be expected in the area

where the cracking initiated. The peak strain was measured up to CPLT levels (ie. 100% DLL at FASS 281.28) and details follow.

Recordings were first taken at low load levels (20%, 50% DLL) and then during the CPLT case; hysteresis was evident and plastic deformation left residual tensile strain (1100 microstrain) in the area where cracking initiates. Figure 17 shows the similarities between chordwise strain distribution on the panel and first box specimen and the full scale wing.

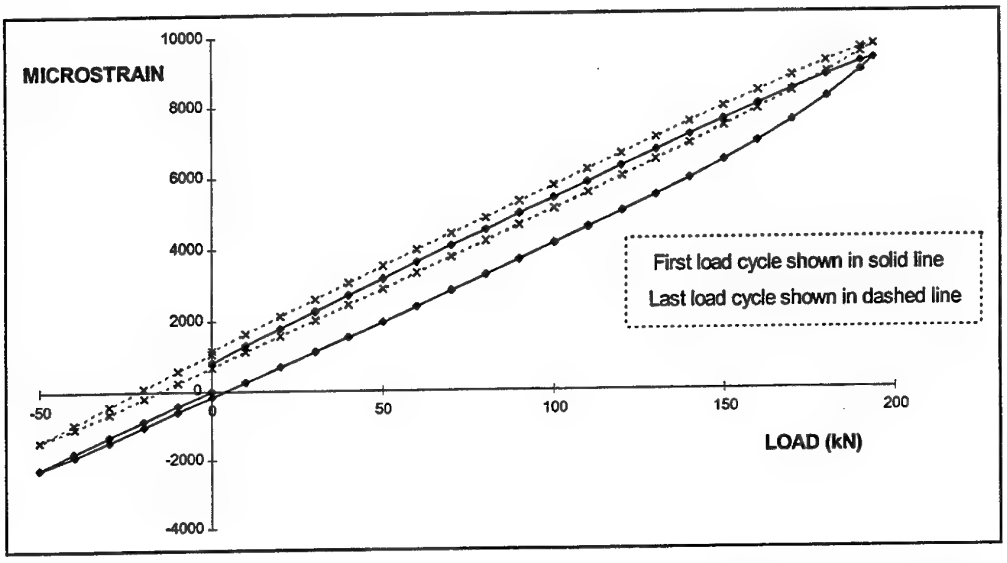

Figure 8. Panel specimen during CPLT load case (strain gauge SO5A-3 at centreline on side representing upper surface of lower wing skin).

Note that there is non-linear deformation in this area (where the cracking initiates) when first loaded above 70% DLL (149 kN). This effect is followed by hysteresis and residual tensile strain of 1100 microstrain.

3.3.2 Patched Panel Specimens

Strain survey tests were undertaken on two cracked, patched panel specimens. The strain gauge layout included some positions used in strain survey tests of a full sized F-111A wing at AMRL[10], and some positions used in the second box specimen.

These tests were done to determine the effect of residual strains from the patch cure and also the variation of strain with temperature (ambient and 80°C).
Refer to section 4.6 for details.

3.4 Fatigue results

3.4.1 Constant amplitude test

An initial conservative test on one patched panel specimen used a constant amplitude loading spectrum of zero to 80% DLL (+1 kN to +176 kN tension).[14]

The specimen did not have a bending restraint attached; out-of-plane deflection was clearly evident. The crack grew immediately upon loading, with failure occurring at a crack length of 190 mm (full panel width) after 7870 cycles.

3.4.2 Block spectrum

The blocked DADTA spectrum was applied to two patched and one unpatched panel specimens.[15] This is also considered to be a severe spectrum when compared[34] to the FALSTAFF spectrum; the unpatched specimen failed after 15.8 equivalent flight hours. The patched specimens' crack length grew from 40 to 78 mm after ~2170 equivalent flight hours. Refer to Figure 19. The repair increases the specimen life by greater than 100 times (2170 ÷ 15.8 = 137.3).

The first patched specimen failed outside the test area at the fastener hole adjacent to the end of the patch. The fastener hole had a crack of approximately 20 mm that was not detected prior to failure. The failure was attributed to the amount of cross-sectional area remaining outside the repaired region, but was indicative of the stress concentration at the end of the patch (as on the aircraft).

The static strength of the second specimen was 312.3 kN (376.7 MPa) with a crack length of 78 mm. This is over 90% of the strength of a patched specimen with a 40 mm crack (312.3 ÷ 342.8 = 0.91), and very close to the DUL of 384 MPa (98%). Another specimen in later tests, with a crack length of 134 mm, reached 97% DUL, indicating good damage tolerance.

3.4.3 Cycle-by-cycle spectrum

The original DADTA information was also analysed to provide a more representative cycle-by-cycle spectrum.[13] This less severe spectrum was applied to all remaining specimens; results are shown in Figure 9 for cracked panel specimens (three patched and three unpatched)[16].

One patched specimen (*FLTP27-12*) had several static strength tests applied after it had endured 30,000 equivalent flight hours (including CPLT cases). At crack lengths between 62 and 63 mm, the DUL (318 kN) was applied nine times with no failure. Then, when the crack was grown to 134 mm (under constant amplitude cycling), the ambient static residual strength was found to be 310.2 kN (97% DUL).

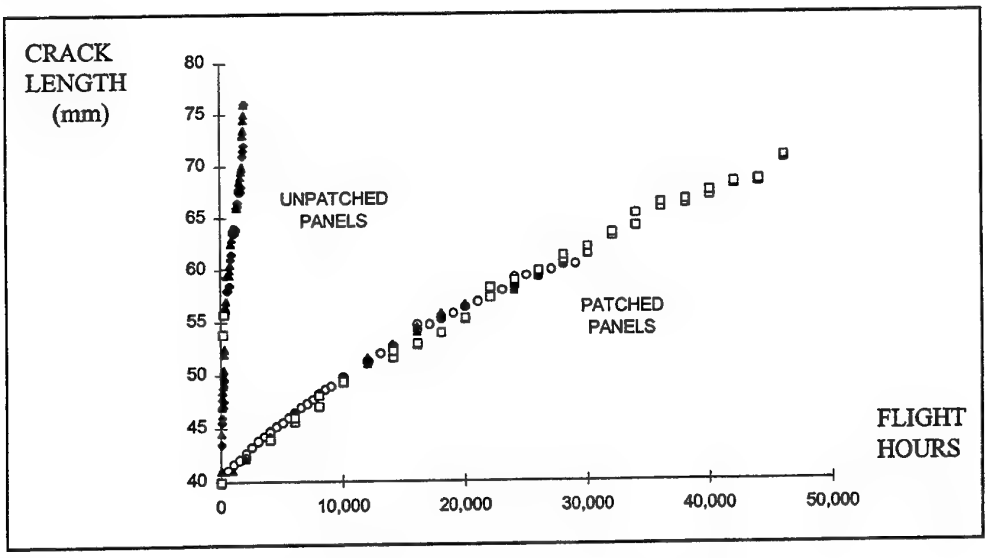

Figure 9. Fatigue crack growth rates using the cycle-by-cycle spectrum

These results indicate a significant improvement in life obtained from the patch repair. 30,000 flight hours approximates 100 years at current RAAF usage rates.

3.4.4 Spectrum truncation effects

At the completion of testing described in section 3.4.3, the crack growth of a patched specimen (*FLTP-16*) was monitored under a constant amplitude loading.[16] This test was to further justify the truncation level (discriminant) used in the cycle-by-cycle spectrum, by finding the level at which crack growth is no longer detectable.

The constant amplitude loading was reduced in several steps of 20% until, at the level where the load range was +1 kN to +28.6 kN, the crack growth was considered stopped (less than 1.0×10^{-9}m/cycle). The truncation level in this spectrum is 5 ksi (34.5 MPa), equivalent to 28.6 kN for a panel specimen (34.5 x 0.829 = 28.6). This compares well with truncation levels of 10 ksi from other tests[33] at AMRL.

3.5 Crack initiation

3.5.1 Specimen results

The USAF specimen clearly shows multiple initiations from the upper surface leading to a semi-circular crack front which penetrates the lower surface before finally becoming a through crack approximately 40 mm long. Pre-cracking of all early specimens were able to generate similar final crack profiles from an introduced EDM flaw. Four panel specimens, with a bending restraint but without an introduced flaw, were tested[23] under the cycle-by-cycle spectrum to investigate crack initiation and growth rates.

In all cases, there was multiple crack initiation consolidating into one dominant crack with a varying degree of asymmetry ; the cracks were not always parallel to FASS 281.28. This behaviour is similar to that in the USAF specimen. The crack growth rate was similar in all specimens from initiation to a through thickness crack.

3.5.2 Damage Tolerance Assessment Based on Crack Initiation Results

Using a combination of simplified, conservative analysis and the panel specimen test results[23], a Damage Tolerance Assessment (DTA) for the cracking at FASS 281 can be carried out as follows:

Assuming $K_c = 46\ \text{MPa}\sqrt{m}$ (as per Reference 1), the critical crack length a_{crit} at DLL is calculated as follows:

For $\sigma = 256$ MPa (at DLL)
and $K = K_c$
$= 46\ \text{MPa}\sqrt{m}$
$= \sigma\sqrt{\pi a_{crit}}$ (assuming a through thickness centre crack in an infinite sheet)
$\Rightarrow a_{crit} = 0.0103$ m $= 10.3$ mm
$\Rightarrow 2\,a_{crit} = 20.6$ mm

This value corresponds well with data for the unpatched panel specimen *FLTP69-1*, where the crack tore from 26 to 52 mm during a CPLT load case.

From laboratory tests[23], the RAAF eddy current NDI technique was able to readily detect the crack at a length of 2a = 6 mm. This detection was from the side representing the lower surface of the lower wing skin, when the crack was only open to the side representing the upper surface.

From Figure 10, the average crack growth curve gives a growth time from 2a = 6 mm to 2a = 20 mm of approximately 2,000 hours. These results therefore support an inspection interval for this region of approximately 1,000 hours.

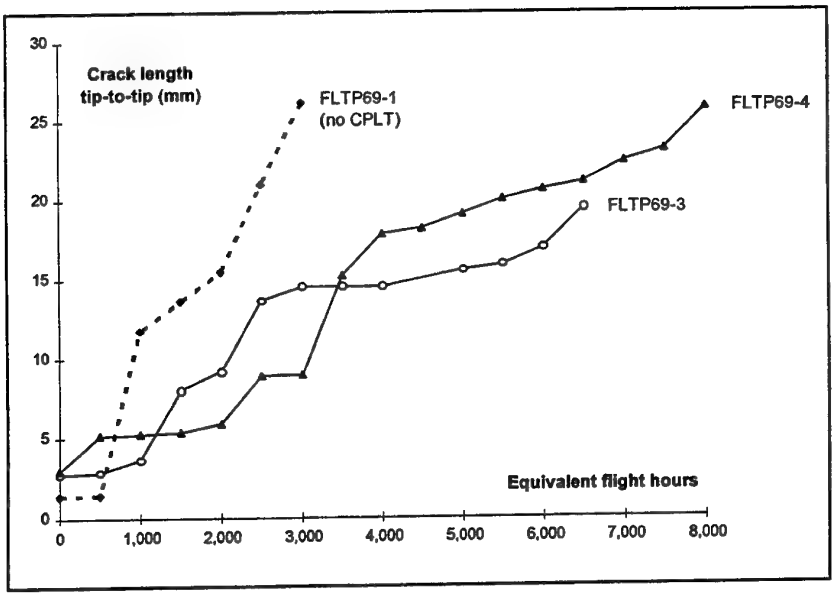

Figure 10. Crack growth of panel specimens from first initiation under the cycle-by-cycle loading spectrum.

Note that the specimen *FLTP69-1* was not loaded quite the same as the others; the CPLT load cases were omitted until the last block (whereupon it failed).

Using the above data, an estimate of the time to grow from the minimum measurable size (6 mm) to the critical crack length (20.6 mm) ranges from 1800 to 5500 equivalent flight hours.

3.6 Temperature and frequency effects

3.6.1 Crack propagation sensitivity

The influence of temperature on crack propagation behaviour in the aluminium structure, after the application of a bonded composite patch, may be explained by three factors[35] :

- The effective stress ratio, R, is increased due to the residual thermal stresses induced from the difference between the patch bonding cure temperature and the subsequent operating temperature. In this case it is tension in the aluminium wing skin structure and compression in the boron/epoxy repair patch.
- The patching efficiency changes because the properties of the FM73 adhesive vary considerably with temperature. With increasing temperature, the shear modulus, G, and yield strength, τ_p, of the adhesive are reduced

and thus patching efficiency is reduced. However, the residual thermal stresses will reduce as the operating temperature increases.

- The crack propagation properties of the alloy may change with temperature. For this aluminium alloy, reference values[36] of fracture toughness show a decrease of approximately 6%, or less, as the temperature increases from -40°C to +23°C.

The potential influence of loading frequency on patched crack propagation is due to the time spent at high loads, where the adhesive is loaded into the plastic region. Creep effects are more likely to occur at elevated temperatures where the modulus and yield point of the adhesive are reduced.

3.6.2 Thermal residual strains

The residual strain in patched specimens was estimated from strain gauge measurements on a panel[23] and box[17]. The second box specimen (*Box 2*) and one panel specimen (*FLTP69-4*) were instrumented with an array of electrical resistance strain gauges, both on the boron patch and the aluminium structure. Refer to Appendices 2, 3 and 4 for gauge locations. With the specimen under no externally applied load, the voltages from the strain gauges were recorded prior to the bonding of the patch and also afterwards.

After the patch adhesive cured, the residual strain induced in the boron patch ranged from -551 to -1330με in the centre of the box patch (and -442 to -1000με for the patch on the panel specimen). At the tapered ends of the patch the strain variation in the patch over the ply terminations was slightly higher, but erratic in adjacent gauges (-464 to -1468με in the box and -439 to -1149με in the panel).

After the test loading on the panel specimen was completed (18,000 simulated flight hours at ambient temperature and 80°C), the residual strain had changed ; in the centre it ranged from -411 to -804με and at the ends of the patch it was now tension, ranging from +11 to +1301με.

Temperature tests[23] were also undertaken on unloaded samples of the materials (fitted with electrical resistance strain gauges) used in this substantiation program. Strain gauge measurements were taken at temperatures ranging from -15°C (freezer), to +84°C (oven). Results for the linear response were as follows :

Aluminium Panel (alloy 2024-T851) = 21.54 με/°C
Patched Panel (same on both sides) = 13.12 με/°C
Boron/Epoxy patch laminate (0° ply direction) = 2.93 με/°C

These compare well to reference values[4] of thermal co-efficients of expansion for Aluminium (23×10^{-6}/°C) and uni-directional boron laminate (4.1×10^{-6}/°C).

This data indicates that residual strain in either type of specimen (box or panel) at ambient temperature (23°C) induced by the cure at 80°C can be calculated as follows for a ΔT of 80 - 23 = 57°C :

With both boron and aluminium components heated to 80°C, prior to bonding, the strain induced by the temperature change is

Aluminium	(21.54 με/°C) x 57 = 1228 με
Boron	(2.93 με/°C) x 57 = 167 με

- This compares well with far-field strain data measured from panel specimen *FLTP69-4* at 80°C (gauge #15 on aluminium panel indicates 1225 με, and gauge #13 on boron patch indicates +137 με).

With both boron and aluminium components then at the ambient temperature of 23°C, after the bonding process was completed, the strain induced by the temperature change is

Aluminium	1228 - (13.12 μE/°C) x 57 = 480 με
Boron	167 - (13.12 μE/°C) x 57 = -581 με

- This compares well with far-field strain data measured from panel specimen *FLTP69-4* at 23°C (gauge #15 on the aluminium indicates +531 με, and gauge #13 on the boron indicates -548 με).

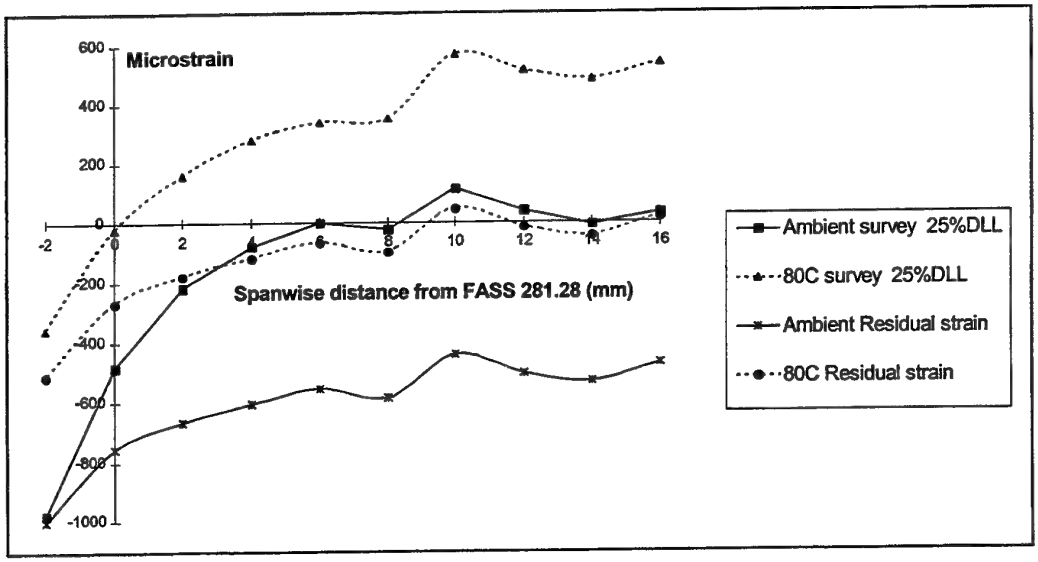

Figure 11. Strain distribution in the boron patch at 25% D.L.L. on panel specimen FLTP69-4.

The strain distributions, shown above, include all residual strain from the patch cure and the temperature effect on the strain gauges at 80°C. The values of residual strain are shown for reference. The residual strain at ambient temperature was measured with the specimen fully assembled, but resting on a flat surface; the residual strain at 80°C is calculated relative to those ambient values with an offset correction, given from Figure 12.

The total strain in the centre of the patch at 80°C is clearly much higher (by approximately 500 microstrain) than that at ambient temperature under the same loading conditions. However, when allowing for the effects of residual strain and temperature, the net strain distribution at 25% DLL (ie compared to zero load) is very similar in both cases (23°C and 80°C).

The three axial-type electrical resistance strain gauges on panel specimen *FLTP69-3* were recorded at temperatures -15, +23 (ambient), +50, +60, +70, +80, +82 and +84°C, with no load applied to the specimen. The "panel lower" description refers to the gauges on the boron patch. Two other items were gauged similarly to the panel specimen to give comparisons at the same temperatures; a sample of the boron patch laminate had a longitudinal and lateral pair of gauges, and fractured panel specimen *FLTP27-4* (unpatched) had a strain gauge fitted in the same location as gauge #15 on panel specimen *FLTP69-3*. As a baseline measurement to determine the temperature effect on the gauges, each type of gauge was attached to a piece of silica glass (which has approximately zero co-efficient of expansion) and tested separately.

Temp (DegC)	ε_Al	ε_panel lower longitudinal	ε_panel lower lateral	ε_panel_upper longitudinal	ε_Boron longitudinal	ε_Boron lateral
-15	-850	-518.37	-558.48	-510.11	-119.07	-608.18
50	560	370.90	448.38	372.68	124.38	520.14
60	788	497.00	572.60	493.43	132.91	604.79
70	991	611.05	700.57	616.85	153.29	744.25
80	1198	734.48	830.67	738.93	167.74	873.01
82	1240	758.09	854.29	762.55	170.63	873.90
84	1282	783.05	875.23	791.51	175.00	900.19

Figure 12. Corrected strains (x 10^{-6}) for axial-type strain gauges.

The recorded strains were corrected firstly by zeroing them relative to the average values at ambient temperature (23°C) and then secondly by correcting for the thermal effects of the gauges themselves; at 80°C, this is +582με for the axial-type gauges and +488με for the strip-type gauges).

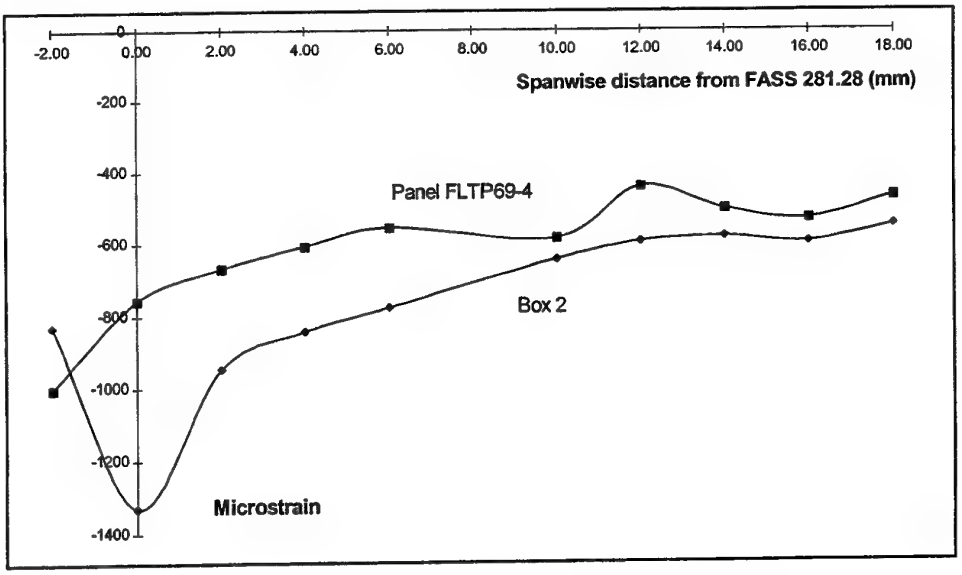

Figure 13. Residual strain distribution at zero load, ambient temperature

The residual thermal strain distribution in the boron patch is similar for both box and panel types of specimens. The residual strain in the aluminium structure would be expected to be a similar level but tensile. This significant level of residual tensile strain in the local region of the crack could be expected to have the effect of increasing the stress ratio, R.

The residual strain in the boron patch on the panel specimen was not at its maximum at the centre; this can be partly explained by the accidental 0.5 mm offset of the patch from the centreline and also because the pre-crack in the panel did not initiate on the centreline, but approximately 2 mm from it. The residual strain at the centre of the boron patch is greater in the second box specimen[24] (*Box 2*) than in the panel specimen (*FLTP69-4*).

3.6.3 Temperature and loading frequency tests

The sensitivity of crack growth rate to the temperature (and hence stress ratio, R) is not predicted to be significant because other tests[35] performed at -40°C showed no observable change compared to ambient temperature.

Two patched panel specimens (*FLTP69-3, FLTP69-4*) were loaded under the cycle-by-cycle spectrum, initially at ambient temperature (23°C) at 5 Hz. The effects on crack growth rate by elevated temperature (80°C) and low frequency (0.5 Hz) are shown in Figures 14 and 15.

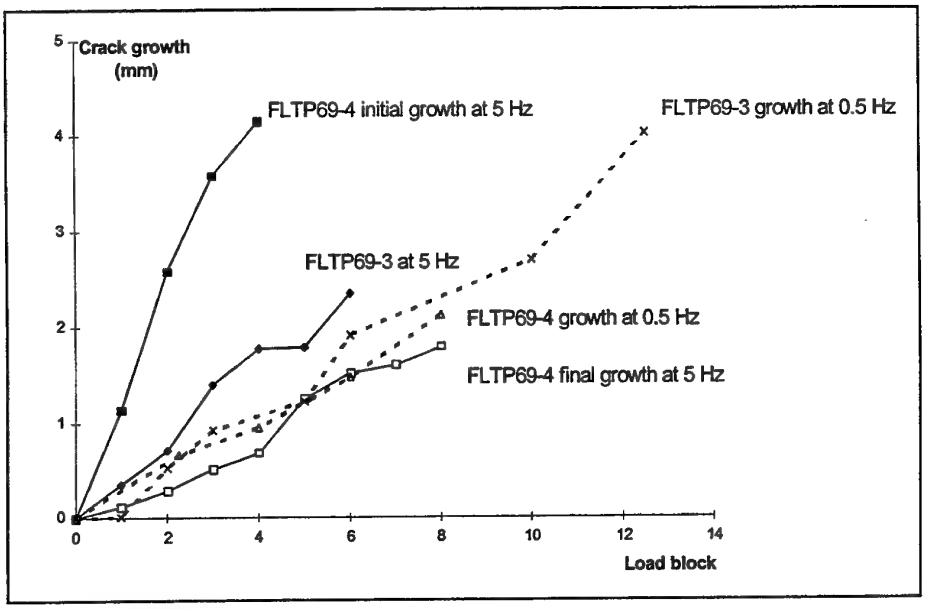

Figure 14. Crack growth comparisons at ambient temperature in specimens FLTP69-3 *and* FLTP69-4.

Crack growth rate comparisons can be made using linear regression of the relevant data :

Slope of ambient growth at 5.0 Hz = 0.24, 0.39 and 1.08 mm per block (500 hrs)
Slope of ambient growth at 0.5 Hz = 0.31 and 0.26 mm per block (500 hrs)

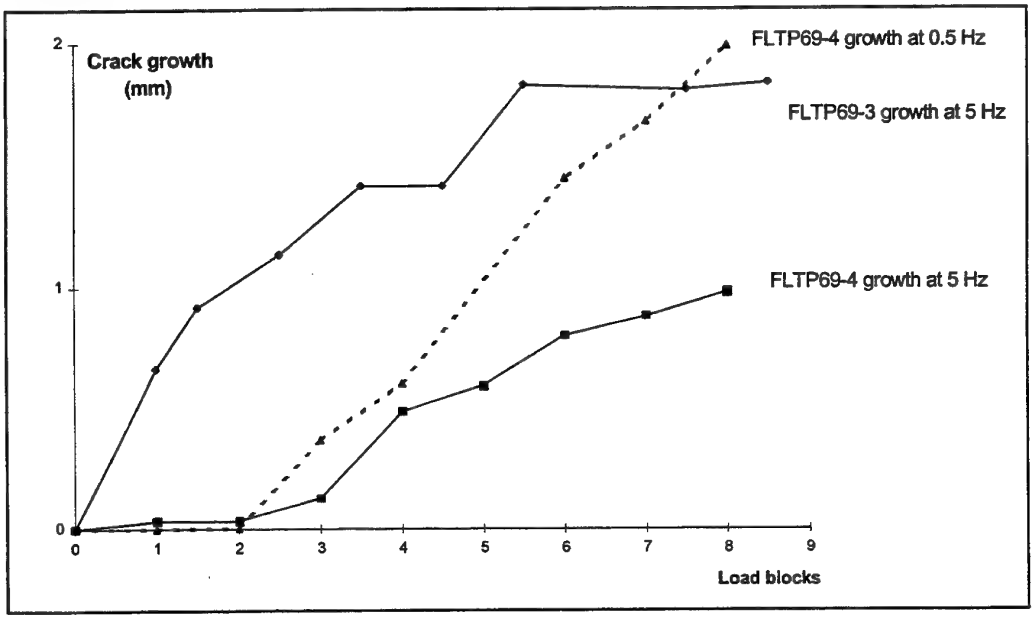

Figure 15. Crack growth comparisons at 80 ℃ in specimens FLTP69-3 *and* FLTP69-4

Crack growth rate comparisons can be made using linear regression of the relevant data :

Slope of 80°C crack growth at 5.0 Hz = 0.14 and 0.19 mm per block (500 hrs)
Slope of 80°C crack growth at 0.5 Hz = 0.28 mm per block (500 hrs)

- The crack growth rate at 0.5 Hz does not show any influence from the test temperature (0.31 and 0.28 at ambient and 0.28 at 80°C).
- The crack growth rate at 5.0 Hz is slower at 80°C, than it is at ambient (0.14 and 0.19 at 80°C and 0.24, 0.39 and 1.08 at ambient).

These variations in crack growth rate are not considered significant and might be expected within experimental variation for two specimens. The average value of crack growth of 0.72mm per 1000 hours is consistent with earlier ambient temperature tests[15] performed on panel specimens at 3 and 5 Hz.

3.7 Summary of panel specimen tests

- The strain distribution in the panel specimen is similar to that of the full-scale wing, but the secondary bending is greater in the panels (more conservative).

- Crack initiation in skin panel specimens (with no deliberate notch) occurred at multiple sites, and did not always begin at the line representing FASS 281.28, nor progress parallel to it. This asymmetric nature is also evident in the specimen taken from a USAF fleet aircraft. The crack-front progression pattern of specimens loaded under a representative cyclic load spectrum is similar to that on the USAF specimen. The crack can be detected from the lower surface using standard RAAF eddy current NDI techniques when only 6 mm long on the upper surface. This suggests an inspection interval of approximately 1000 hrs for an unpatched aircraft in the RAAF fleet to find a crack between 6.0 and 20.6 mm in length.

- Thermal residual strains in the panel specimen (due to the cure cycle of the bonded boron patch) were found to be significant ; levels were as high as 1150 microstrain in the boron patch. After 18,000 equivalent flight hours of cyclic loading, including tests at elevated temperature, the residual strains were still evident in the central region of the patch, but at a reduced level (up to 300 microstrain less). However, at the ends of the patch, the residual strain had changed from compression to tension by as much as 1450 microstrain.

- The static strength of a specimen (40 mm crack) is less than DLL unless it is patched; its residual strength is then not affected by hot (+83°C) or cold (-16°C) temperatures. The residual static strength of a patched specimen with a large crack was 90% of one with a small crack, but at 105°C this was still greater than the reduced DLL for the 110°C design case.

- The boron patch repair did not prevent crack growth in the patched panel specimens but growth was very much slower than in unpatched specimens. The fatigue life of the unpatched specimen was extremely short, especially under the severe block spectrum. Under the cycle-by-cycle spectrum, the crack length grew far more slowly; at a loading frequency of 0.5 Hz, there was no change in growth rate when the operating temperature was increased from ambient (23°C) to 80°C, but at 5.0 Hz, the crack growth rate appeared to be slower at 80°C.

- Non-destructive inspection (using ultrasonic techniques) of the patch bond during the tests showed signs of disbonding, approximately 6 mm wide, in the immediate region of the crack. Standard RAAF eddy current NDI techniques can also measure the crack length through the patch.

4. Box Specimen testing

4.1 Box specimen description

The box specimen is designed to incorporate the out-of-plane support and thermal mass provided by the wing spars and is large enough to install a full-size repair patch. The specimen test section is an assembly of two skins and three webs (representative of the Forward Spar, Forward Auxiliary Spar (FAS), and Centre spar). Each skin contains a test section that is a full-scale replica (other than skin curvature profile) of the fuel flow passage in the lower wing skin at FASS 281.28. The specimen material is Aluminium 2024-T851, machined to final size, and hand finished by polishing to aid crack measurement.

The fastener spacing and nominal size is the same as the aircraft, however, the first specimen has clearance fit holes to ensure no shear load transfer between the skin and webs. The second specimen has interference fit fasteners along the middle web (FAS); the same as that used on the aircraft (0.25" diameter countersunk head Taper Lok bolts). A "tongue" adaptor, to mate with the grips of the testing machine, makes up of each end of the box so that loads can be applied to the specimen.

The introduction of the crack defect into the specimen skins was achieved by creating a notch in centre of the side representing the inner surface of the lower wing skin using Electro Discharge Machining (EDM). The specimen is partially assembled with all three webs but only one skin and then loaded under cyclic tension loading until a crack appears at each end of the notch and grows to the required length on both surfaces. The crack initially grows on the inner surface but eventually breaks through the thickness to give a semi-circular crack front. As the crack grows further it becomes more like a simple "through crack" with a similar crack length on both surfaces of approximately 48 mm. The specimen is then disassembled and the procedure is repeated with the other skin, before being reassembled in preparation for bonding of

the boron patches. This crack defect is similar in shape to that in the specimen supplied from the USAF F-111G wing.

The different crack length used in the two specimen types (panel and box) is due to the information received during the testing program. The initial estimate of the crack size in RAAF aircraft F-111C (A8-145) was 40 mm; for consistency, this value was used for all panel testing. A later measurement of the crack showed it to be 48 mm and this value was used for the later tests involving the box specimens.

Patching was applied (after pre-cracking) to each skin's side representing the outer surface of the lower wing skin after it was carefully cleaned, grit blasted and treated with an adhesion promoter to ensure a good bond surface. Full-sized repair patches were made with 14 plies of Boron/Epoxy pre-preg fibre composite 5521-4.[11] The pre-cured patch is bonded using FM-73 adhesive cured at 80° Celsius. The bonded patches on both skins of a fully assembled box specimen were cured simultaneously, before non destructive inspection (NDI) of the patched areas to confirm patch and bond integrity.

24 channels of strain gauges were fitted to the skins and central web of the first box specimen[17] (before any pre-cracking or patching) including positions identical to those in the full scale wing strain survey.[10] Prior to the beginning of fatigue loading on the completed specimen, a further ten channels were fitted to the patch outer surface on both skins.

35 channels of strain gauges were fitted to the second box specimen, including 34 on one of the patches before it was bonded, so that thermal effects of the cure cycle could be investigated. After the patches were bonded, a further 5 strain gauges were fitted to one of the skins around the patch and one was also fitted to the centre of the outside web.

The test specimen geometry, configuration and strain gauge locations are shown in Appendix 4.

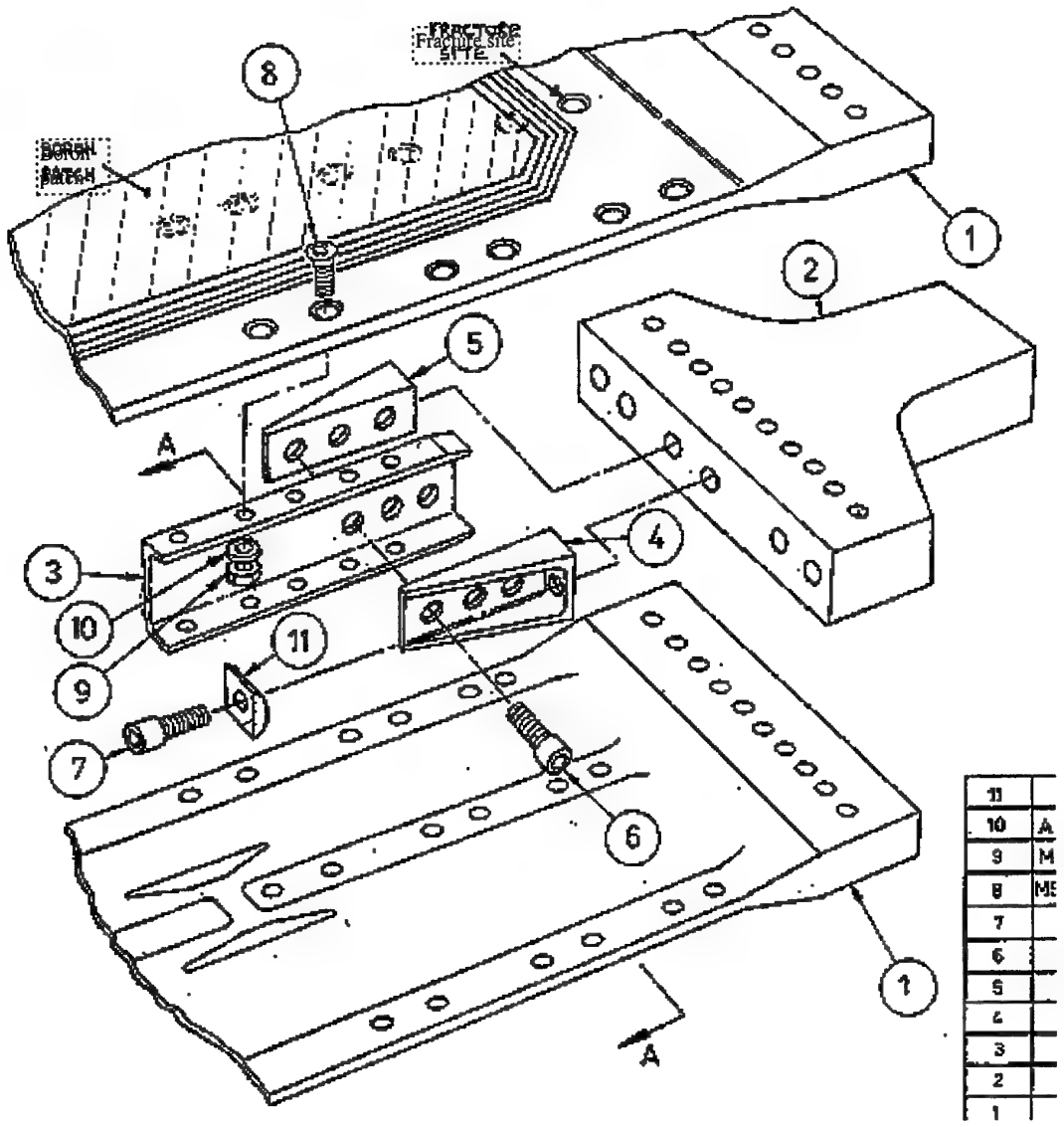

Figure 16. Box specimen - exploded view

4.2 Strain survey results

4.2.1 First box specimen

The tests involving static load strain surveys were carried out conventionally on the specimen initially prepared with one skin and three spars. Each test began with a recording of data at nominal zero load and then at each increase in load increment up to the maximum value (50% DLL). Data was also recorded as the load was decreased from the maximum via the same increments and then a final zero reading was taken.

The results from the first box specimen[17] are compared with those from the panel specimen[8] and the full-scale wing[10] in Figure 17, shown below. All three structures were neither cracked nor patched.

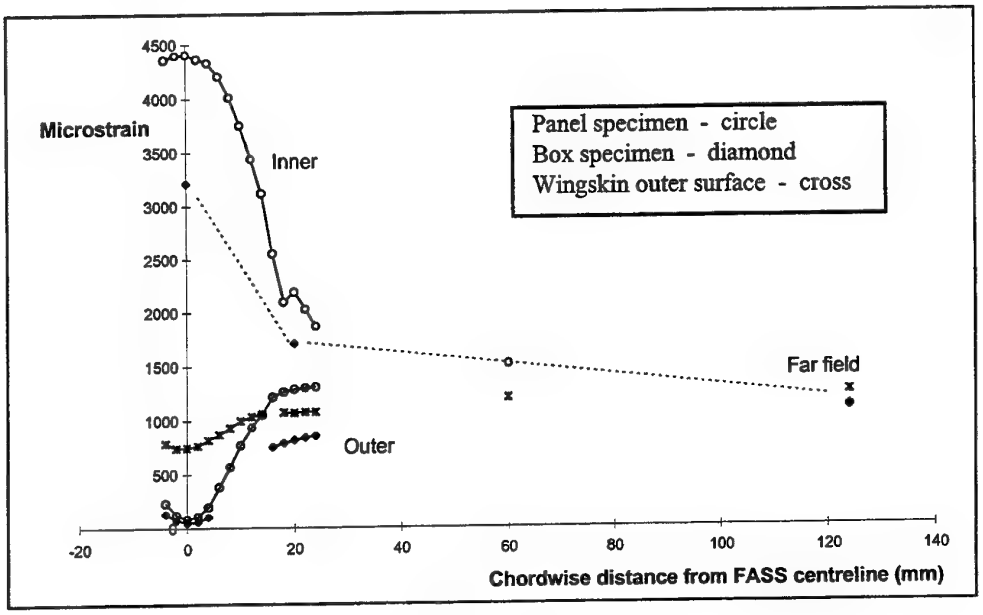

Figure 17. Strain distribution chordwise at 50% D.L.L.

The far field strains are similar in the box specimen (1100 με) and the full sized wingskin (1150 με) but both are lower than in the panel specimen (1500 με). A similar difference is evident for the strain on the side representing the inner surface of the wing skin at the centreline, (3200με for the box specimen and 4400με for the panel specimen). The distribution of strain across both specimens is consistent, but both specimen types show considerably more secondary bending than the full scale wing. This is partly because the specimens were manufactured to the design skin thickness (3.7 ± 0.1 mm) compared with the test wing, which is 4.2 mm thick in this area. It is also partly due to the fact that the bending restraint in the panel specimen is not identical to the full-scale wing.

A strain survey was done before fatigue testing began with the box specimen fully assembled, pre-cracked and patched; results are shown below in Figure 18.

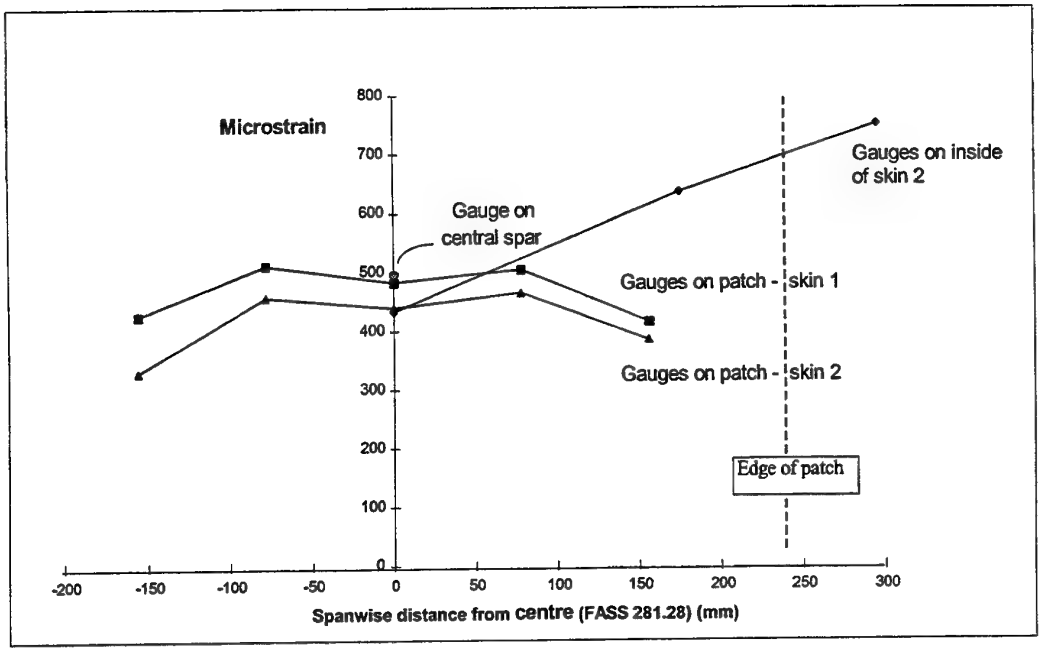

Figure 18. Strain distribution at 20% D.L.L. of fully assembled box specimen prior to fatigue spectrum loading.
Refer to Appendix 4 for strain gauge labelling and locations.

At the centre of the specimen, the strain in the patch, the skin panel and the central spar/web are within 10%, indicating that the load is evenly distributed between the three elements. Most of the load transfer from the aluminium skins into the boron patch has occurred within 90 mm from end of the patch. There is no evidence of load transfer within 70 mm of either side of the crack at the centre (FASS 281.28).

4.3 Fatigue results

4.3.1 First box specimen

The specimen was loaded under the block spectrum at ~1.5 Hz with halts for NDI inspection at end of each block of 8,628 cycles (100 equivalent flying hours)[17].

The cracks in both skins of the specimen continued to grow immediately. During the fifth load block a partial tear-down found 5 of the 12 fasteners attaching the web fittings to the tongue adaptor fittings had failed due to tensile fatigue loads. Several other fasteners no longer had the specified torque and there were fretting products on most of the faying surfaces. The specimen was re-assembled and a repeat of the static strain survey showed no significant change to the one performed before cycling commenced. Specimen failure occurred just prior to the end of the eighth load block at

a skin fastener location adjacent to the end of the boron patch - an unexpected crack had propagated across the full width of the skin on side 1.
NDI inspection of the failure site led to suspicions about the other three similar fastener locations; further inspection found cracks in the bores of the skins at all three locations.

Without disassembly of the specimen, a FAST (Focal plane Array for Synchronous Thermography) camera imaging of surface strain was used to generate a contour plot of the sum of the principal strains. The FAST investigation of the intact skin (side 2) looked at the areas in the centre of the patch and also at the zone at the end of the patch and the adjacent fastener. See section 6 for details.

After 800 equivalent flight hours of the blocked loading spectrum, the crack length in each skin was 70.5 and 71 mm. Ultrasonic A-scan NDI carried out in the vicinity of the crack gave "indications" of disbonding for a spanwise distance of about 6 mm and about 70 mm in the chordwise direction. However, subsequent teardown inspections were not conclusive as to whether such a disbond really existed or not. The stress analysis carried out for this repair[9,25] indicates that plastic deformation is expected in the adhesive in the region of the crack. It also indicates that if a disbond was to occur, then the local stresses and strains would be relieved and the disbond would not propagate. The test results are consistent with this analysis.

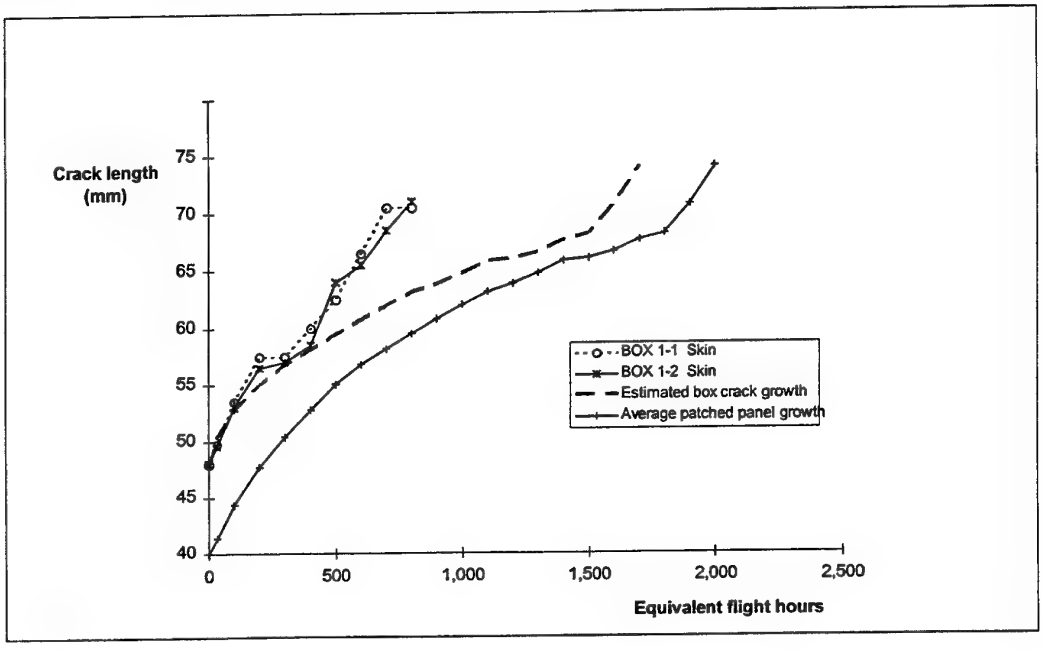

Figure 19. Specimen crack growth under blocked spectrum loading.

The patched and pre-cracked panel specimens were tested from 40 mm crack lengths (compared to 48 mm in the box specimen), so an equivalent predicted crack growth curve for the box specimen is calculated by translating (horizontally) the average growth curve to the match the values at 48 mm to obtain the dashed curve shown in Figure 19, above.

The two box specimen data curves are for each skin panel (box 1-1 and box 1-2) on the specimen. The correlation between the values predicted from previous tests on panel specimens, and these test results is good for the first 10 mm of crack growth.

4.3.2 Second box specimen

The specimen was loaded under the cycle-by-cycle spectrum at ~1.5 Hz with regular halts for NDI inspection[17]. Initially, crack measurement (via eddy current techniques) and verification of bondline integrity (via A-scan ultrasonic techniques) were performed after each block of 36,273 turning points (500 equivalent flight hours), but when performance became stable, it was extended to be done after each CPLT (ie. 4 blocks). A sequence of four blocks and the CPLT, followed by NDI inspection, was able to be completed within 24 hours, allowing almost continuous running.

The 48 mm cracks in both skins of the specimen began to increase immediately and the noise emitted from the specimen under load was similar to the previous test. Despite this aural evidence of fretting, there was no loosening of fasteners and no change in strain distribution after 24 blocks (= 12,000 flight hours) or 44 blocks (= 22,000 flight hours). NDI inspections were done at the 4 fastener locations in the centre spar adjacent to the ends of the patch where cracks were found in the first specimen, one of which led to failure. Interference fit Taper-Loks were used at all fastener locations along the centre spar of the second specimen, even though their countersunk shear heads were sub-flush. The specimen skins had already been countersunk for larger tension head fasteners at all locations. No cracks were detected at these locations even after disassembly at the end of the test. After 40 load blocks there were indications of disbonding at the ends of the patches; these areas enlarged slightly with continued loading, then stopped. The largest region was a maximum of 15 mm of degraded bondline along the width of one end of skin 2.

After 30,050 equivalent flight hours of the cycle-by-cycle loading spectrum, the crack length in skin 1 was 78.0 mm and in skin 2 was 73.5 mm. Ultrasonic A-scan inspection of the repair patch indicated a disbond (38 mm long by 4 mm wide) over the middle of the crack and also around the ends of the patch, to a small extent.

The specimen was then statically loaded to failure in tension. Two fasteners, connecting the end fittings to the tongue adaptors, failed during this test before both skins fractured at the fastener line just beyond the end of the boron patch at a load of 91.4% D.U.L. After disassembly, it was discovered that four other bolts had failed from fatigue cracks during the cyclic testing. Fretting was severe between the steel fittings and aluminium spars/skins and most fastener holes in the spars were elongated. Two

of the end fittings were severely distorted locally under the tension bolt head by the static loading.

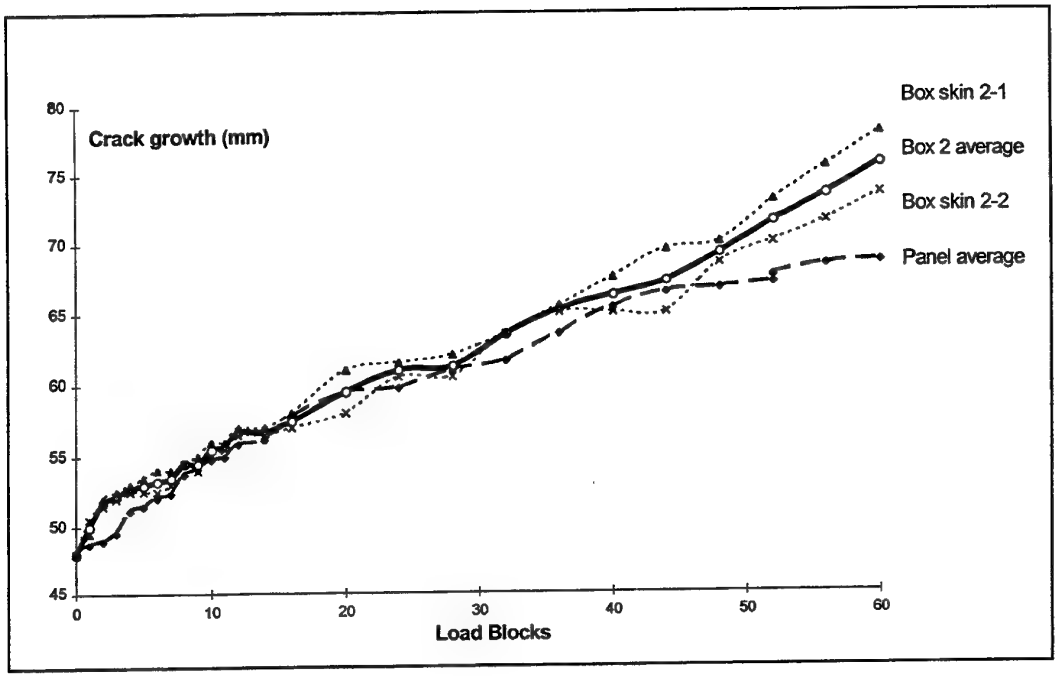

Figure 20. Second Box Specimen post-repair crack growth

The patched and pre-cracked panel specimens were tested with crack lengths starting from 40 mm (compared to 48 mm in the box specimen), so an estimated crack growth curve for the box specimen was calculated as per Figure 9.

The box specimen data curves are for each skin panel (Box 2-1 and Box 2-2) on the specimen and also for their average values. Correlation between predicted values and test results is good between 48 and 70 mm.

Note :
1) One load block is equivalent to 500 flight hours.
2) This crack growth zone extends into the adjacent integral side stiffeners. The crack tips reach the fillet radii when the crack length is approximately 55 mm and reach the lands of the stiffeners at 70 mm.

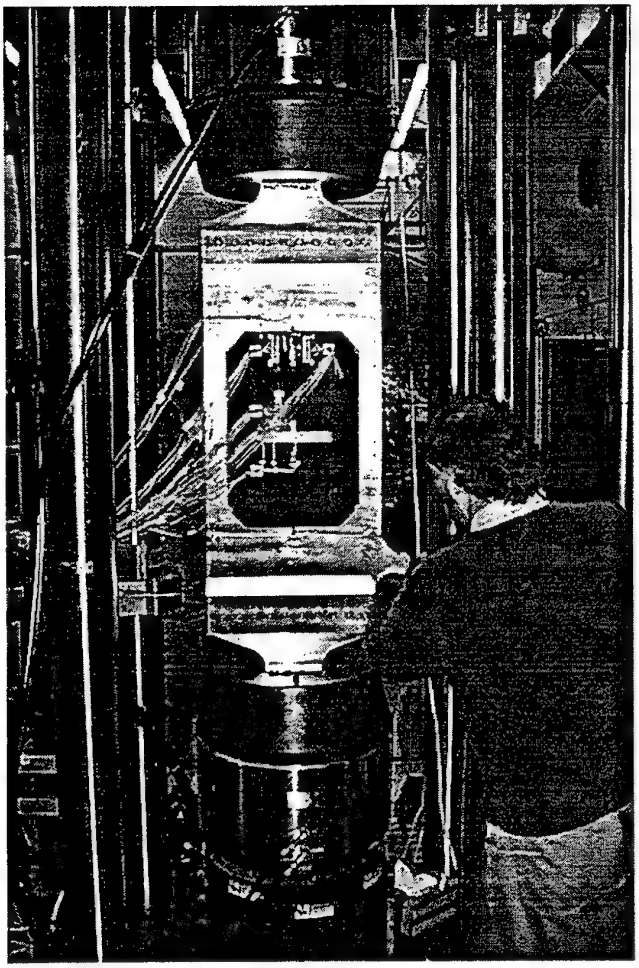

Figure 21. View onto side 1 of second box specimen in 2 MN testing machine showing strain gauge array and fracture line below end of patch.

4.4 Summary of box specimen results

The test results show general similarities in the strain distribution between the full-scale wing test, the "skin-only" panel specimen and this built up box specimen. However, there is a significant difference in the magnitude of strains at the centre of the specimen. Factoring the applied loads based on the cross-sectional area did not show good agreement between the far field strain levels of the different specimens. This is believed to be due to the significantly greater level of secondary bending present in the test specimens (panel and box) compared with the test wing. The difference is due to the significantly thicker skin of the test wing (4.19 mm) compared with the blueprint thickness of the specimens (3.6 - 3.8 mm). This significance has been demonstrated using FE models with varying skin thickness[20].

Fatigue crack growth, under the block spectrum, in the first box specimen was comparable to the panel specimens from the beginning (at 48 mm tip-to-tip) until the crack length reached approximately 55 mm. Note that the crack growth zone extends into the adjacent integral side stiffeners. The crack tips reach the fillet radii when the crack length is approximately 55 mm and reach the lands of the stiffeners at 70 mm.

that the distance between the fillet radii of the stiffeners on either side of the central area (where the crack initiates) extends between 55 and 70 mm. The box specimen failed unexpectedly at a fastener location in one skin. The fastener was just beyond the end of the repair patch, outside the test section. After 800 equivalent flight hours of a severely conservative loading spectrum, the crack lengths were 70.5 and 71 mm, with indications that the patch disbonded over this length for a width of approximately 6 mm. Destructive inspections carried out after the end of the test were inconclusive as to the presence and extent of any disbonding over the crack; it was certainly no greater than 6 mm in width.

Fatigue crack growth in the second box specimen, under the cycle-by-cycle spectrum, was consistent with the three panel specimens. After 30,050 equivalent flight hours of this more representative loading spectrum, the crack lengths were 78.0 and 73.5 mm, with the NDI indicating the patch was partially disbonded over 40 mm of this length for a width of approximately 4 mm . There was some degradation of the patches at their ends, with NDI C-scans, after the static test to failure, indicating disbonds extending up to 15 mm from the ends.

5. Fracture Toughness Tests

Tests were undertaken[18] to assess the conservatism in the value of plane strain fracture toughness, K_{Ic} (MPa$\sqrt{m}$) used in the original analysis of the patch repair. Six specimens were manufactured from aluminium alloy 2024-T851, using material taken from a F-111 wing at AMRL (3 off) and from the 25 mm plate used to manufacture the panel and box specimens (3 off). The aircraft wing skin thickness in the repair area is nominally 3.7 ± 0.1 mm.

The stress intensity specimen is an edge-cracked plate 90 mm wide with a crack 20 mm long. The thickness of specimens made from wing material was 3.2 mm, and those from the 25 mm material were 3.7 mm. The specimens were loaded under uni-axial tension increasing from zero at 1.0 kN per second until failure occurred.

Since the fracture surface of all specimens showed a plane stress type failure (rather than a plane strain failure) K_{Ic} is not valid for this thickness; the stress intensity factor K_c is used instead.

In a thickness of 3.2 mm, the average K_c was 57.3 MPa$\sqrt{m}$
In a thickness of 3.7 mm, the average K_c was 60.9 MPa$\sqrt{m}$

This gives an average value for K_c of 59.1 MPa$\sqrt{m}$

The original analysis for the repair[21] used a value of K_{Ic} = 46 Mpa$\sqrt{m}$ (42 ksi$\sqrt{in}$)

6. Failure modes

6.1 End fastener failure analysis

Several test specimens failed outside the test area. Two panel specimens failed under static loading in the tapered region close to the grips of the testing machine[14]. These were attributed to stress concentrations due to the changes in geometry. Referring to Figure 5, the cross-sectional area at section 2 (less than 828.6 mm^2) is smaller than that at section 1 (829.2 mm^2), when there is no crack. Also, a repaired panel specimen (patched and cracked) may be weaker outside the patch, without some treatment of the area in section 2. Later panel specimens were then polished and shot-peened in the area of section 2 to prevent this type of failure.

Under cyclic loading, there were two failures (one in panel *FLTP27-9* and one in the first box specimen) at the fastener hole immediately outside the end of the repair patch. Both were cyclic loaded under the blocked fatigue spectrum and both had clearance fit fasteners installed. The fracture surface of the box specimen is shown below in Figure 22 (the fracture surface of the panel is similar). The geometry of this part of the box specimen is similar to the repaired aircraft A8-145 - the patch terminates 10 mm from the centre of a 6.25 mm (nominal 0.25 inch) diameter, 100° countersunk, fastener hole. Note that there are different fasteners used ; clearance fit on the first box specimen and all the panel specimens, and interference fit on the second box specimen and the aircraft. The second box specimen also failed at this region during a static test to failure but there was no evidence of a fatigue crack initiating from any holes.

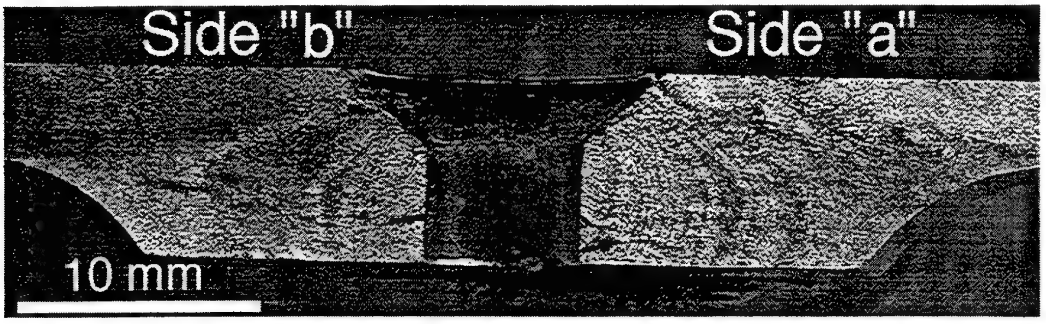

Figure 22. View onto fracture surface of first box specimen

Fatigue crack growth is clearly visible emanating from the bore of the fastener hole. A clearance fit fastener was used at this location and there is residual adhesive remaining in the bore (the fasteners were intentionally bonded in position). The crack proceeded to failure before it progressed past the end of the countersink. It was not detectable prior to failure, even with 45 degree angled eddy-current probe techniques. Similar sized cracks were evident at the other three similar fastener locations after the fasteners had been removed.

The fractographic analysis[19] showed that a subsurface flaw initiated the crack shown in Figure 22. The use of clearance fit fasteners (in lieu of interference-fit fasteners as per drawing) was not thought to have contributed to the crack growth. The more likely cause is the stress concentration induced at the end of the repair patch (approximately 15%) superimposed on the stress concentration around the fastener hole.

After failure of the first box specimen, a the FAST (Focal plane Array for Synchronous Thermography) thermoelastic imaging system was used to assess the strain variation on the specimen. The image shown below in Figure 23 shows the distribution of the sum of the principal surface strains.

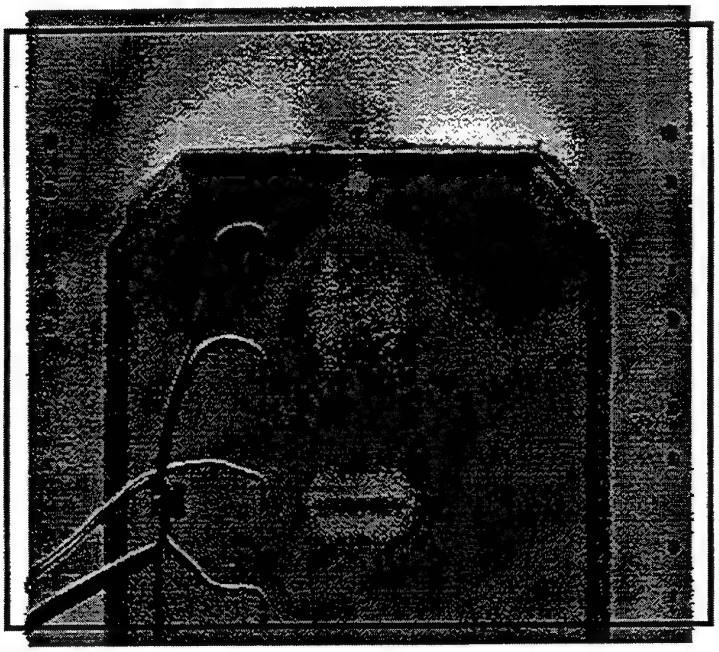

Figure 23. FAST scan - View onto Box 1, skin 2 repair patch after 800 equivalent flight hours. Spanwise load axis is vertical in this view. Lighter shaded areas have higher levels of surface strain.

The increased strains are clearly evident in the central region in the lower part of this view, where the crack location is shown by the darker line. The fastener location adjacent to the end of the patch is in an area of unusual strain distribution ; a small

crack (subsequently found after disassembly) is in the hole bore but this is not highlighted by a light shaded high stress zone.

6.2 Fractographic analysis

6.2.1 Aluminium sections

A comparison of the fracture surface of the USAF specimen and three of the AMRL panel specimens is shown in Figure 24. The crack front can be clearly seen growing from multiple initiations on the inner surface which join into a semi-circular crack. After breaking through the outer surface it becomes a through crack approximately 40 mm long. A replica of the final through crack can be obtained in test specimens by the introduction of a semi-circular EDM notch followed by constant amplitude cyclic tension loading. The multiple initiations for the crack were evident in panel specimens, that had no EDM notch, loaded under the cycle-by-cycle spectrum[19].

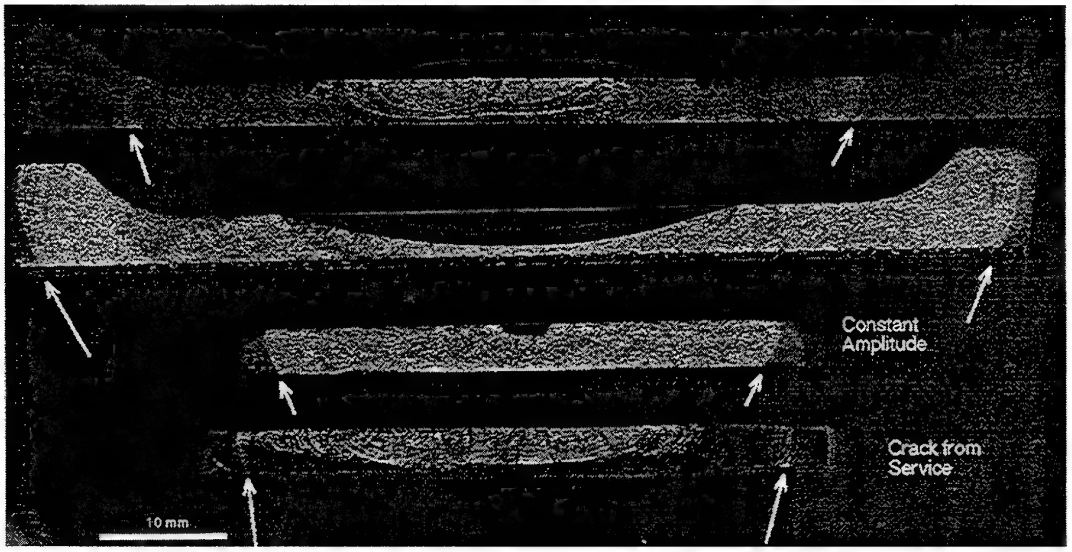

Figure 24. Fracture surfaces (from top down)

- *Panel specimen with no crack initiation, under cycle-by-cycle spectrum to failure.*
- *Panel specimen with large EDM notch, constant amplitude to 40 mm, then patched before failure under cycle-by-cycle spectrum.*
- *Panel specimen with small EDM notch, constant amplitude loading to 40 mm, then static load to failure.*
- *USAF fleet wing specimen (approximately 40 mm tip-to-tip).*

6.2.2 Boron fibre epoxy composite

The first patched panel specimen loaded cyclically without a bending restraint, failed due to large secondary bending loads with delamination failure of the repair patch.

All other panel specimens that did not fail outside the test section, had a consistent failure mode. As the crack in the central area of the aluminium specimen grew, the adhesive became unbonded over a width of approximately 6 mm and a length similar to that of the crack. Due to the limited accuracy of the NDI measurements of the disbond, it could not be determined during the testing if the crack tip was consistently leading the disbond or vice versa.

The fracture mode of panel specimens was often a clean fracture of the repair patch (no delamination) adjacent to the fracture in the aluminium adherend. Fractography shows crack growth in the adhesive very similar to that in the aluminium adherend (in Figure 25 below), but cannot determine what the failure sequence is between fibre fracture, adhesive disbonding/fracture, and cracking in the aluminium adherend. It is proposed that the crack growth in the aluminium matches that in the adhesive, since the final fracture tear begins at exactly the same place in both materials[22].

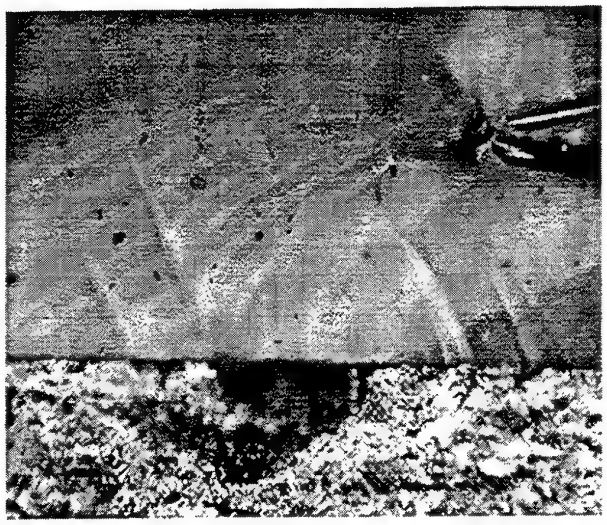

Figure 25. Crack growth in adhesive layer.

The crack front is parallel to progression lines and perpendicular to chevrons. (aluminium shown darker, in lower third of picture, below interface).

The dark mark in the top right of the picture is the non-structural carrier cloth for the adhesive. Post fracture analysis showed evidence of some crack growth in the adhesive initiated at the intersections of the warp and weft of the carrier cloth.

7. Discussion

Several experimental techniques were developed during the test program:

Bending restraint
The panel specimens were initially designed to be only loaded in tension, due to the assymetrical cross-section. During constant amplitude cycling at 5 Hz (to obtain a reasonable test duration), out-of-plane bending instability was severe. The panel design was modified to incorporate fasteners at the same pitch and size as those in the aircraft wing. The fasteners were used to clamp a bending restraint to the panel and thus increase stability, also allowing the application of limited compression loads in the fatigue spectra. The restraint had slotted holes and teflon strips were fitted between it and the panel to allow axial movement; this limited the restraint to act against out-of-plane movement only.

The strain distribution in the panel and box specimens tended to have more severe secondary bending (conservative) but were generally representative of that in the full-scale wing and the F.E.M.

Polishing / Peening
Premature failures out of the test section on panel specimens were prevented by polishing and peening with glass beads to induce a residual compression zone.

Interference fit fasteners
The fastener used in the aircraft lower wing skin is the Taper Lok (0.25" diameter, 100° countersunk head). These were used in the second box specimen to make it more representative of the aircraft wing and to reduce the amount of fretting that occurs between the skin and webs with clearance fit bolts. Both the box specimens failed at the fastener hole outside the test section, however, when Taper Loks were installed in the second specimen, there were no fatigue cracks initiated (as in the first box); simply net section failure during the residual strength test.

FAST
Thermographic analysis using the FAST system was carried out on both panel and box specimens to visualise the global strain distribution. Areas of interest were the far-field areas (to compare with strain gauge readings), the high stress zones around fastener holes and changes in geometry such as radii of stiffeners. It was very effective in highlighting general effects, but difficult to quantify the results.

NDI
Several NDI techniques were used during the testing. After repair patches were applied to specimens, ultrasonic C-scans were performed to check bond integrity, while during cyclic loading tests, hand-held A-scans were performed to determine the extent of bondline degradation.

Using eddy current equipment, the crack growth in the adherend could be measured to within ±1 mm through the thickness of the patch. During the crack initiation tests on unpatched panel specimens, the crack can be measured (using standard RAAF eddy current equipment and techniques) from the far side (representing the outer surface of the lower wing skin) even when it is only 6 mm long and 2 mm deep.

Crack measurement
With visual access to the crack, a stereo microscope (mounted on a travelling slide and fitted with a digital micrometer) was used. Measurements of crack length from tip-to-tip at different magnifications (x8, x16, x40) with hand held lighting could be done consistently to ±0.005 mm

Repair patch geometry
The full size patch was applied to the box specimens. A smaller version of the patch was fitted to the panel specimens; it was still a 14 ply laminate with the same termination geometry but the width was reduced (from 325 mm to 190 mm) and the overall length was reduced from 470 mm to 285 mm. The assumption that the panel specimens would still behave like the box specimens (crack growth rate is quite similar) has shown to be true, thus indicating a conservative patch design.

Other important results to come out of this test program are :

- The static strength of a specimen (40 mm crack) is less than DLL unless it is patched; its residual strength is then not affected by hot (+83°C) or cold (-16°C) temperatures. The residual static strength of a patched specimen with a larger crack was 90% of one with a small (40 mm) crack, but at 105°C, it is still greater than the reduced DLL for the high temperature (110°C) case.
- Crack growth in repaired specimens is not zero, but an acceptably low consistent rate at frequencies between 0.5 and 5.0 Hz, and temperatures between 23°C and 80°C. The growth rate is similar in panel and box specimens.
- The actual value for fracture toughness of the wing material was found to be higher than that used in the original repair design analysis.

8. Conclusion

The structural integrity of a bonded boron epoxy repair to a fatigue crack in the lower wing skin of an RAAF F-111C aircraft has been fully substantiated through testing of two levels of representative specimens. The testing has demonstrated that the repair:

a) Adequately restores static strength under all design load and temperature cases
b) Has sufficient durability and damage tolerance.

The static strength of the wing was estimated to have been reduced to below Design Limit Load due to the presence of a 48mm chordwise fatigue crack, and this was confirmed by a residual strength test on a cracked, unpatched panel specimen. The application of the boron epoxy patch has been shown to restore the static strength to above Design Ultimate Load for three load cases, ie elevated temperature (+110^{0}C), ambient room temperature and reduced temperature (-40^{0}C). The original design had been checked against these three conditions.

The durability of the repair, and its effectiveness in reducing the crack growth rate were also demonstrated to be adequate. Crack growth behaviour in the panel and box type specimen was consistent, slow (less than 1.0 mm per 1,000 spectrum hours typically) and easily detectible using conventional NDI methods. Residual strength was shown to be unaffected by crack growth, and the crack growth rate did not vary significantly with changes in temperature or frequency of loading. The repair was demonstrated to perform effectively for more than 30,000 simulated flight hours.

The damage tolerance of the repair was demonstrated in several ways. Repairs applied to the specimens were known to contain typical manufacturing imperfections and the system displayed sufficient tolerance to these. The patches applied to the panel specimens were significantly shorter than the full scale patch and still performed very well, thereby effectively further demonstrating a tolerance to significant damage. In all cases, there were indications of local debonding at the crack face and the repairs were tolerant of this.

The testing program established a reasonable estimate of the crack growth behaviour for an unpatched wing. When combined with a demonstration of the sensitivity of the ultrasonic NDI technique being used by the RAAF to inspect for cracks on fleet aircraft, this information supports an inspection interval for the fleet of 1,000 flight hours (the current wing bay service interval).

In conjunction with independent analyses[6,9,20], these test results successfully substantiate the bonded repair to the port lower wing skin of RAAF aircraft A8-145. This work also confirms the validity of the RAAF Engineering Standard[4] C5033 as a basis for the design and application of bonded composite repairs to thin-skin metallic structure.

9. Acknowledgements

The following people are gratefully acknowledged for their skilled contributions to specimen design, preparation, testing and fractography :

P. Penhall	K. Lemm	B. Ashcroft	G. Camov	M. Engellener
G. Collins	D. Rowlands	P. Cox	M. Ryan	R. Koning
C. Rey	P. Ferrarotto	N. Goldsmith	R. Pell	L. Mirabella
J. Ayling	P. Hayes	O. Beninato	N. Hall	J. Roberts
I. Stoyanovski	C. Niessen			

The authors are grateful for the advice, guidance and support from Dr L.R.F. Rose and Dr. A.A. Baker throughout this program.

References

[1] Rose, L.R.F., Callinan, R.J., Baker, A.A., Sanderson, S. and Wilson, E.S., 1995, *Design validation for a bonded composite repair to the F-111 lower wing skin.* Proceedings PICAST2-AAC6, P. 331-336, Institution of Engineers, Melbourne, Australia,

[2] Baker, A.A., Jones, R., (eds)., 1988, *Bonded Repair of Aircraft Structures.* Martinus Nijhoff.

[3] Baker, A.A., 1994, *Bonded Composite Repair of Metallic Aircraft Components - Overview of Australian Activities.* AGARD Specialists Meeting on Composite Repair of Military Aircraft Structures, Seville, October 3 - 5.

[4] Anon, 1994, *Composite Materials and Adhesive Bonded Repairs.* RAAF Engineering Standard C5033, Draft.

[5] Penhall, P., 1994, *Validation testing for bonded repair to F-111C (A8-145),* Statement of Requirements, AMRL file SE5/53/1/2.

[6] Callinan, R.J., Sanderson, S., 1995, *Analysis of RAAF Bonded Repair to F-111 Lower Skin, Part 1 - Uncracked Analysis.* AMRL Report (M1/9/136).

[7] Boykett, R., 1995, *Strain survey on panel test specimen of F-111C lower wing skin at FASS 281.28.* AMRL Structures Laboratory Report Number 2/95.

[8] Boykett, R., 1995, *Detailed strain survey of panel test specimen representing F-111C lower wing skin at FASS 281.28.* AMRL Structures Laboratory Report Number 5/95.

[9] Callinan, R.J., Sanderson, S., Keeley, D., 1996, *3D FE Analysis of a Bonded Repair to an F-111 Wing*. Proceedings ACAM96, Institute of Engineers, Melbourne, Australia.

[10] Hayes, P., 1994, *F-111 Outer wing strain survey at fuel flow hole in forward auxiliary spar*. AMRL Structures Laboratory Report Number 1/94.

[11] RAAF drawing 501WG94020000 *Boron / Epoxy repair patch.*

[12] Anon. RAAF, 1994, *Design approval package for bonded repair to aircraft A8-145.*

[13] Walker, K., Swanton, G., 1995, *Static and fatigue test loading development for F-111C bonded composite repair substantiation,* AMRL report to be published.

[14] Boykett, R., 1995, *Bonded boron patch repair validation on representative specimens of wing cracks in F-111C aircraft.* AMRL Structures Laboratory Report Number 1/95.

[15] Boykett, R., 1995, *Repair validation fatigue tests of F-111C wing skin panel specimens.* AMRL Structures Laboratory Report Number 4/95.

[16] Boykett, R., 1995, *The cycle-by-cycle fatigue testing of F-111C lower wing skin repair specimens.* AMRL Structures Laboratory Report Number 10/95.

[17] Boykett, R., 1995, *The validation testing of a F-111C lower wing skin repair box specimen.* AMRL Structures Laboratory Report Number 9/95.

[18] Boykett, R., 1995, *Stress intensity factors for thin aluminium alloy 2024-T851.* AMRL Structures Laboratory Report Number 3/95.

[19] Goldsmith, N., 1995, *AMRL preliminary report of fractographic analysis of failure sites in F-111C box specimen and panel specimen.*

[20] Keeley, D., Callinan, R.J., Sanderson, S., 1996, *An Investigation into the sensitivity to small geometry changes in an F-111C lower wing Finite Element Model.* AMRL Technical Report in preparation.

[21] Anon., 3 May 1994, *Design approval for the interim repair of F-111C Wing S/N A15-5,* under RAAF minute ASI/4080/14/A8-12Pt4(35).

[22] Pell, R., 1996, *AMRL preliminary report of fractographic analysis of boron, adhesive and aluminium failure sites in F-111C box specimen and panel specimen.*

[23] Boykett, R., 1996 *Crack growth tests in F-111C lower wing skin repair panel specimens.* AMRL Structures Laboratory Report Number 10/96.

[24] Boykett, R., 1996 *The validation testing of F-111C lower wing skin repair box specimens.* AMRL Structures Laboratory Report Number 9/95.

[25] Davis, M.J., Kearns, K.J., Wilkin, M.O., March 1995, *Bonded repair to cracking in primary structure : a case study.* Proceedings PICAST2-AA6, P. 323-330, Institution of Engineers, Melbourne, Australia.

[26] McHenry, H.I., Key, R.E., 1968, *The F-111 Logic: familiar materials: proven processes.* Metal Progress. 93, No. 3, p.62-68.

[27] Broek, D., 1989, *The practical use of fracture mechanics.* Kluwer, Dordrecht.

[28] Anon, 23 September 1994, *F-III LOWER WING SKIN - BOX BEAM SPECIMEN ASSEMBLY.* ARL Drawing number 66345-A0, Revision 1.

[29] Anon, 1988, *Standard test method for measurement of fatigue crack growth rates.* American Society for Testing and Materials ASTM E 647-88a .

[30] Fuchs, H.O., Stephens, R.I., 1980, *Metal fatigue in engineering,* John Wiley and Sons, USA.

[31] Anon, *Damage tolerant design handbook,* Metals and Ceramics Information Centre, MCIC-HB-01, Columbus, Ohio, USA.

[32] Anon, November, 1990, *MIL - HDBK - 5F.*

[33] Baker, A.A., August 1996, *Fatigue studies related to the certification of composite crack patching for primary metallic aircraft structure.,* FAA-NASA Symposium on continued airworthiness of aircraft structures, Atlanta, USA.

[34] Raizenne, M.D., Benak, T.J., Heath, J.B.R., August 1994, *Bonded composite repair of thin metallic materials : Variable load amplitude/temperature cycling effects.,* LTR-ST-1979, Institute for Aerospace Research, Canada.

[35] Baker, A.A., October, 1994, *Bonded composite repair of metallic aircraft components - Overview of Australian activities.,* 79th AGARD Structures and Materials Panel on "Composite repair of military aircraft structures.", Seville, Spain.

[36] Brown, W.F., Mindlin, H., et al., 1992, *Aerospace structural metals handbook,* Volume 3, Code 3203, Figures 3.03721 and 3.03722.

Appendices

Appendix 1

Specimen summary

Specimen Serial No.	Specimen Description	Loading Conditions	Failure information
FLTP27-1	cracked, patched	ambient, static	342.8 kN = 414 MPa
FLTP27-2	cracked, no patch	ambient, static	206.2 kN = 249 MPa
FLTP27-3	cracked, patched	fatigue 75%DLL, no restraint, ambient	crack length 190 mm after 7870 cycles
FLTP27-4	no crack or patch	First strain survey, then ambient, static	320.9 kN = 387 MPa fail outside test area
FLTP27-5	cracked and patched	+110°C, static	347.2 kN = 419 MPa failed outside test section, crack 55 mm
FLTP27-6	cracked and patched	-40°C, static	356.9 kN = 431 MPa
FLTP27-7			
FLTP27-8	cracked, no patch	blocked spectrum, ambient	Failed after 15.8 flight hours (@ 130.6 kN)
FLTP27-9	cracked, with patch	blocked spectrum, ambient	Failed at hole outside test area at 2133 flight hours (crack 77.5 mm @ 158.5 kN)
FLTP27-10	cracked, with patch	Blocked spectrum then static residual strength test, ambient	At 2200 flight hours (crack length 77.9 mm 312.3 kN = 377 MPa)
FLTP27-11	no crack or patch	Detailed strain survey	not failed
FLTP27-12	cracked, with patch	cycle spectrum, ambient	Crack length 62.2 mm at 30,000 hrs. 134 mm at failure (310.2 kN = 374 MPa)

Figure 26. Summary of test specimen configurations and results

Specimen Serial No.	Specimen Description	Loading Conditions	Failure information
FLTP27-13	cracked, no patch	cycle spectrum, ambient	Failure after 315 hours at 161.7 kN
FLTP27-14	cracked, no patch	cycle spectrum, ambient	Failure after 1941 hours at 160.4 kN
FLTP27-15	cracked, no patch	cycle spectrum, ambient	Failure after 2000 hours at 179.8 kN
FLTP27-16	cracked, with patch	cycle spectrum, ambient, then tests for truncation levels	No failure. Crack length 62.2 mm at 30,000 hrs. Truncated at 28.6 kN = 5 ksi
FLTP27-17	cracked, with patch	cycle spectrum, ambient, then static test at 110°C.	Crack length 62.1 mm at 30,000 hrs, 69.4 mm at 50,000 hrs. Failure at 110°C at 204.7 kN (246 MPa)
FLTP69-1	not cracked	crack initiation	Failure after 13,297 hrs, at 171.6 kN (=207 MPa) Crack length 52.94 mm
FLTP69-2	not cracked	crack initiation	Machine malfunction - failure when crack length 12 mm
FLTP69-3	cracked, with patch	crack initiation, then cycle spectrum (hot and slow effects).	Failure at fastener under patch at 151.6 kN (=183 Mpa) after 13,296 hrs. Crack length 50.2 mm
FLTP69-4	cracked, with patch	crack initiation, then cycle spectrum (hot and slow effects).	No failure. Crack length 51.4 mm after 18,000 hrs

Figure 26. (cont.) Summary of test specimen configurations and results

Specimen Serial No.	Specimen Description	Loading Conditions	Failure information
BOX-1 (Side 1)	cracked, with patch	Strain survey, block spectrum loading	Crack length 71 mm after 800 hrs. Failed outside test section.
BOX-1 (Side 2)	cracked, with patch	Strain survey, block spectrum loading	Crack length 71 mm after 800 hrs. Failed outside test section.
BOX-2 (Side 1)	cracked, with patch	Strain survey, cycle spectrum loading, then static residual strength test	Crack length 78.5 mm after 30,060 hrs. Failed at 2044 kN (353 MPa) outside test section.
BOX-2 (Side 2)	cracked, with patch	Strain survey, cycle spectrum loading, then static residual strength test	Crack length 73.2 mm after 30,060 hrs. Failed at 2044 kN (353 MPa) outside test section.

Figure 26. (cont.) Summary of test specimen configurations and results

Failure modes evaluation

Panel Specimens

FLTP 27-1

This was a cracked and patched specimen which was tested to failure under static load at ambient conditions. The crack was approximately 40 mm long (tip-to-tip) and failure occurred at a load of 342.8 kN. Given a cross sectional area of 829 mm², this equates to a nominal stress of 414 MPa. Failure mode was mode 1 fracture due to the 40 mm crack, followed by tension overload failure of the boron patch. The comparison with a simplified analytical prediction is as follows:

From an analysis of the repair at ambient conditions under an applied load of 256 MPa (DLL), the stress intensity is given by:

$K_\infty = 29.8 \text{ ksi}\sqrt{inch} \quad = 32.8 \text{ MPa}\sqrt{m}$ (Reference 12)

Assuming that K_∞ is directly proportional to the applied load, and assuming that K_{IC} is equal to 46 MPa$\sqrt{m}$ (as per the original repair design[12]), the failure stress can be estimated as follows:

Failure stress (estimate) = $46 \times \frac{256}{32.8} = 359$ MPa

This compares well with the actual failure result of 414 MPa

FLTP 27-2

This was a cracked specimen with no patch which was tested to failure under static load at ambient conditions. The crack was approximately 40 mm long (tip to tip) and failure occurred at a load of 206.2 kN. Given a cross sectional area of 829 mm², this corresponds to a nominal stress of 249 MPa. Failure mode was mode 1 fracture due to the 40 mm crack. The comparison with a simplified analytical prediction is as follows:

Assume K_{IC} = 46 MPa$\sqrt{m}$. Also assume that we have a through thickness centre crack in a finite width sheet. From Reference 30, K_I is calculated as follows:

$$K_I = \sigma\sqrt{\pi a}\left[\sec\frac{\pi a}{w}\right]^{0.5}$$

a=20 mm (0.02 m), w = 190 mm (0.19 m), $K_I = K_{IC}$ = 46 MPa$\sqrt{m}$

$$\Rightarrow \sigma = \text{Failure stress} = \frac{46}{\sqrt{\pi \times 0.02}\left[\sec\frac{\pi \times 0.02}{0.19}\right]^{0.5}} = 178 \text{ MPa}$$

This is a conservative estimate compared with the actual result of 249 MPa.

FLTP 27-3

This was a cracked and patched specimen which was tested under constant amplitude fatigue cycling from zero to 75% DLL (192 MPa). The crack propagated from an initial size of 40 mm (tip to tip) to the full width of the specimen (190 mm) in 7870 cycles. A comparison with a simplified prediction is as follows:

For the patched, ambient case, K_∞ = 32.8 MPa$\sqrt{m}$ at 256 MPa (DLL)

$\Rightarrow$ at 75% DLL, K_∞ = 0.75 x 32.8 = 24.6 MPa$\sqrt{m}$

From handbook data,[31] the crack growth rate corresponding to ΔK = 24.6 MPa$\sqrt{m}$ is approximately 1.5 x 10^{-2} mm per cycle (this has been extrapolated from the handbook data).

The observed behaviour was growth from 2a = 40 mm to 2a = 190 mm in 7870 cycles. The average growth rate is therefore:

$$da/dN = \frac{\frac{190}{2} - \frac{40}{2}}{7870} = \frac{75}{7870} = 9.5 \times 10^{-3} \text{ mm per cycle}$$

The observed behaviour is thus consistent with expectation based on handbook data.

FLTP 27-4

This was an uncracked, unpatched specimen which was tested to failure under static load at ambient conditions. The failure load was 320.9 kN which corresponds to a nominal stress of 387 MPa (DLL = 256 MPa, DUL = 384 MPa) based on a cross sectional area of 829 mm^2. Failure was due to tension overload and it occurred in "Section 2" of the specimen, ie the run out area close to the grip (see Figure 4).

The yield and ultimate strength values for 2024-T851 are 380 and 480 MPa respectively.[32] Failure of the specimen at a nominal 387 MPa can be explained because a stress concentration due to the curved section of the specimen would be expected. A stress concentration factor, K_T, of approximately 1.2 would be a reasonable estimate for the specimen, and would give a peak stress at failure of 1.2 x 387 = 464 MPa.

FLTP 27-5

This was a cracked and patched specimen which was tested to failure under static load at 110°C. The crack was approximately 40 mm long (tip to tip) and failure occurred in Section 2 (see Figure 4) at 347.2 kN which corresponds to 419 MPa. The failure mode was similar to specimen *FLTP27-4*, indicating that the residual strength for failure at the centre of the specimen (ie the failure location for specimen *FLTP27-1*) exceeded 419 MPa. A theoretical calculation of the K_∞ for the 110°C case was not done because the properties of the FM-73 adhesive have not been determined for more than 82°C. Indeed, the FM-73 adhesive should be extremely flexible at 110°C and the crack bridging efficiency should be significantly reduced. The fact that it appears not to have been may be explained by the fluctuation in temperature across the specimen. The temperature during the test ranged from 83°C near the ends (heat loss was occurring through the grips) to 119.4°C at the centre. The failure in Section 2 indicated that the patch, even at high temperature, had restored the strength of the specimen to at least the uncracked, unpatched condition.

FLTP 27-6

This was a patched and cracked specimen which was tested to failure under static load at -40 deg C. The crack was approximately 40 mm long (tip to tip) and failure occurred at 356.9 kN or 431 MPa. Failure mode was mode 1 fracture due to the 40 mm crack,

followed by tension overload failure of the boron patch. The comparison with a simplified analytical prediction is as follows:

From an analysis of the repair at -40 deg C under an applied load of 239 MPa, the stress intensity is given by:

$K_\infty = 25.1 \text{ MPa}\sqrt{m}$ (Reference 12)

As per the analysis for *FLTP27-1,*

$$\text{Failure stress (estimate)} = 46 \times \frac{239}{25.1} = 438 \text{ MPa}$$

This agrees well with the actual result of 431 MPa.

FLTP 27-8

This was a cracked, unpatched specimen which was subjected to the conservative blocked spectrum loading. Failure occurred at a load of 130.6 kN (157.5 MPa) and was due to mode 1 fracture from the 40 mm crack. An analytical prediction is identical to that for *FLTP27-2,* ie failure stress prediction is 178 MPa. Failure at 157.5 MPa after 1364 cycles of loading and negligible crack growth is therefore within expectation. The 1364 cycles equates to approximately 15.8 flight hours of conservative "blocked" spectrum.

FLTP 27-9

This was a cracked and patched specimen which was subjected to the conservative blocked spectrum loading. The central crack grew from 40 mm (tip to tip) to 77.5 mm in 2,133 flight hours of loading. Failure occurred during the spectrum loading by mode 1 fracture from a second fatigue crack. The second fatigue crack had developed naturally at the fastener hole adjacent to the end of the patch and measured approximately 30 mm (tip to tip). The failure load was 158.5 kN (191 MPa). A simplified analytical prediction is as follows:

$$K_I = \sigma\sqrt{\pi a}\left[\sec\frac{\pi a}{w}\right]^{0.5}$$

a=15 mm (0.015 m), w = 190 mm (0.19 m), $K_I = K_{IC} = 46 \text{ MPa}\sqrt{m}$

$$\Rightarrow \sigma = \text{Failure stress} = \frac{46}{\sqrt{\pi \times 0.015}\left[\sec\frac{\pi \times 0.015}{0.19}\right]^{0.5}} = 208.6 \text{ MPa}$$

This compares well with the actual failure at 191 MPa.

FLTP 27-10

This was an identical specimen (and test) as *FLTP27-9*. On this occasion the central crack grew from 40 mm to 77.9 mm in 2,200 hours of loading. The specimen was then subjected to a residual static strength test at ambient and failure occurred at 312.3 kN (377 MPa). Failure mode was mode 1 fracture due to the 77.9 mm crack, followed by tension overload failure of the boron patch. An analytical prediction for this failure is identical to that presented for *FLTP27-1*. The prediction is failure at 359 MPa which compares well with the actual failure at 377 MPa.

FLTP 27-11

Strain survey specimen.

FLTP 27-12

This was a cracked and patched specimen subjected to the representative cycle-by-cycle spectrum loading. The central crack grew from 40 mm (tip to tip) to 62.2 mm in 30,000 hours. Design Ultimate Load (DUL) of 318 kN was applied and failure did not occur. The specimen was then subjected to constant amplitude cycling until the crack reached 134 mm. A residual strength test was carried out with failure occurring at 310.2 kN (374 MPa, 97% DUL). The analytical comparison is identical to specimen *FLTP27-1* where a failure stress of 359 MPa was predicted. The comparison between predicted and actual failure stress is good.

FLTP 27-13

This was a cracked and patched specimen subjected to the representative cycle-by-cycle spectrum loading. The crack grew from 40 mm to 60 mm in 315 hours and then failed at a load of 161.7 kN or 195 MPa. The failure mode was mode 1 fracture from the central crack. An analytical prediction is as follows:

$$K_I = \sigma\sqrt{\pi a}\left[\sec\frac{\pi a}{w}\right]^{0.5}$$

a=30 mm (0.03 m), w = 190 mm (0.19 m), $K_I = K_{IC} = 46$ MPa$\sqrt{m}$

$$\Rightarrow \sigma = \text{Failure stress} = \frac{46}{\sqrt{\pi \times 0.03}\left[\sec\frac{\pi \times 0.03}{0.19}\right]^{0.5}} = 141 \text{ MPa}$$

The actual failure at 195 MPa therefore compares well with the prediction of 141 MPa.

FLTP 27-14

As per *FLTP27-13* except that the failure load was 160.4 kN (193 MPa) and the crack size was 76 mm. Analytical prediction is:

$$\sigma = \text{Failure stress} = \frac{46}{\sqrt{\pi \times 0.038}\left[\sec\frac{\pi \times 0.038}{0.19}\right]^{0.5}} = 120 \text{ MPa}$$

The actual failure at 193 MPa therefore compares well with the prediction of 120 MPa.

FLTP 27-15

As per *FLTP27-13* and *-14* except that the failure load was 179.8 kN (217 MPa) and the crack size was 76 mm. Analytical prediction is:

$$\sigma = \text{Failure stress} = \frac{46}{\sqrt{\pi \times 0.038}\left[\sec\frac{\pi \times 0.038}{0.19}\right]^{0.5}} = 120 \text{ MPa}$$

The prediction is conservative, but not unrealistic compared to the actual failure.

FLTP 27-16

This was as per *FLTP27-12*. Crack growth behaviour was very similar. The specimen was not tested to failure.

FLTP 27-17

As per *FLTP27-12* and *-16*, except that the spectrum loading was continued for 50,000 hours. Crack growth was consistent with the other specimens. Final crack size was 69.4 mm. The specimen was then subjected to a static residual strength test at 110°C. This time (as compared to *FLTP27-5*) the temperature was more rigidly controlled and varied between 105 and 112°C within the boundary of the patch. Failure occurred at 204.7 kN (246.9 MPa) which is 96 % of DLL. The failure mode was mode 1 fracture of the aluminium followed by tensile overload (and out of plane bending) of the boron patch (see Reference 23 for further details). As stated above, in *FLTP27-5*, an analytical prediction for the K_∞ at 110°C has not been done, however for comparison, the residual strength of an unpatched panel at this crack length is as follows:

$$K_I = \sigma\sqrt{\pi a}\left[\sec\frac{\pi a}{w}\right]^{0.5}$$

a=35 mm (0.035 m), w = 190 mm (0.19 m), $K_I = K_{IC} = 46 \text{ MPa}\sqrt{m}$

$$\Rightarrow \sigma = \text{Failure stress} = \frac{46}{\sqrt{\pi \times 0.035}\left[\sec\frac{\pi \times 0.035}{0.19}\right]^{0.5}} = 127 \text{ MPa}$$

The actual failure at 246.9 MPa indicates that even at this extreme temperature the patch is contributing to reducing the crack tip stress intensity.

FLTP 69-1

This was an unpatched, uncracked specimen which was subjected to spectrum loading until a crack developed naturally. The crack growth curve is shown in Figure 10. Failure occurred during the pre-cracking stage, when the crack was 52.94 mm long, at a load of 171.6 kN. The analysis is the same as that for *FLTP27-1*, giving an estimate of 159.5 Mpa to compare with the test result of 207 MPa.

FLTP 69-2

As per *FLTP 69-1* except that unfortunately the specimen was destroyed by an unintended compression overload before a significant amount of data could be obtained.

FLTP 69-3

Prepared as per *FLTP 69-1*; the crack growth curve is shown in Figure 10. Both these specimens were patched before loading at different frequencies and temperatures. Failure occurred at 80°C at a load of 151.6 kN (=183 MPa) from a unforeseen crack approximately 30 mm long at a fastener hole under the end of the patch. Using the same analysis as for FLTP27-17, the predicted failure is at 211 Mpa which is a good agreement with the test result.

FLTP 69-4

As per FLTP69-3, but was not taken to failure; the crack growth curve is shown in Figure 10.

Box Specimens

BOX-1

The first box specimen was subjected to spectrum loading under the severe "blocked" spectrum. Failure occurred outside the test section from a crack at the first fastener outboard from the end of the patch. Cracks emanated from both sides of the hole. The crack size was approximately 1.0 inch long (tip to tip, including the hole diameter). The failure load was 916.7 kN.

Given a cross sectional area for the box of 5,791 mm², the nominal stress at failure was therefore 158.3 MPa, or 23 ksi. Assuming a centre crack in an infinite sheet, the stress intensity can be estimated as follows:

$$K = \sigma\sqrt{\pi a} = 23\sqrt{\pi \times 0.5} = 28.8 ksi\sqrt{inch} = 31.7 MPa\sqrt{m}$$

Given that the K_C for the material with a skin thickness of 4.2 mm has been estimated at 46 MPa$\sqrt{m}$, it can be assumed that a lower value would apply for the area where this crack occurred (about 8 mm thickness). Additionally, stress concentration, finite width and load transfer effects would be expected to increase the actual stress intensity. This failure is therefore considered to be within expectations.

BOX-2

The second box specimen was subjected to 30,000 simulated flight hours of spectrum loading under the "cycle-by-cycle" spectrum. Static failure occurred outside the test section during the residual strength test, at the section through the first fastener holes outboard from the end of the patch. No fatigue cracks were detectable on the fracture surface. The failure load was 2044 kN.

Given a cross sectional area for the box of 5,791 mm², the nominal stress at failure was therefore 353 MPa, or 51 ksi. Assuming a centre crack the size of the fastener hole (0.25 inch diameter) in an infinite sheet, the stress intensity can be estimated as follows:

$$K = \sigma\sqrt{\pi a} = 51\sqrt{\pi \times 0.125} = 31.9 ksi\sqrt{inch} = 35.2 MPa\sqrt{m}$$

Given that the K_C for the material with a skin thickness of 4.2 mm has been estimated at 46 MPa$\sqrt{m}$, it can be assumed that a lower value would apply for the area where this crack occurred (about 8 mm thickness). Additionally, stress concentration, finite width and load transfer effects would be expected to increase the actual stress intensity. The two box specimen failures are within 10% of each other and therefore considered to be within expectations.

Appendix 2

Panel specimen

Geometry

Skin panel specimens contain a test section that is a full-scale replica of the F-111C aircraft's fuel flow passage in the lower wing skin at FASS 281.28.

The specimen material is Aluminium 2024 - T851 and is machined to final size with no curvature, whereas the aircraft skin is machined, brake-formed to get a chordwise curvature, then chemical - milled to final size before assembling and shot-peening of the outer surface.

Specimen geometry is shown in Appendix 3 shows the boron patch and the crack defect location.

The panel specimen design was later modified to allow for compression cyclic loading; it could have a bending restraint attached to minimise the amount of out-of-plane deflection when the asymmetric cross-section is loaded. The bending restraint is shown in Appendix 3 and is crudely representative of the aircraft wing's spar cap. Although the restraint is attached to the specimen at the same fastener pitch as on the aircraft, it is designed so that no axial load is transferred by having slotted holes in the restraint and teflon spacers to allow elongation of the specimen. The eight (later six) fasteners that attach the bending restraint are bonded into the panel specimen with adhesive under the countersunk heads and in the recessed slots to prevent rotation of the fasteners after the boron patch has been bonded onto the specimen.

Specimen preparation

The panel specimen is hand finished in two areas after being manufactured by polishing out machining marks and scratches with P1200 wet and dry paper. This polishing is done in the central area on both surfaces to assist visual monitoring of crack growth and is done at each end of the test section on both sides, as shown in Figure 4.

The polishing at the ends of the test section is followed by shot peening the masked area to reduce the likely premature failure of the specimen via cracks initiated at the change in cross-section. This type of "Section 2" failure occurred twice in early tests before this treatment was done. The shot-peening is done under manual control of a compressed air jet containing hollow glass spheres.

Specimen pre-cracking

The introduction of the crack defect into the specimens was done by creating a notch in the side representing the inner surface of the lower wing skin using Electro Discharge Machining (EDM). This notch does not extend to the opposite surface ; for the first few panels, it was a slit 0.1 mm wide, 1.0 mm long and 0.5 mm deep, but later was changed

to a semi-circular slit 0.1 mm wide and 35.0 mm long and extends to a maximum depth of 3.5 mm. The second shape was chosen to hasten the pre-cracking process once early tests showed the validity of the profile.

Without the bending restraint attached, the specimen is loaded under cyclic tension loading until cracks appear at each end of the notch. The loading continues until the crack is grown to the required length from each end of the notch on both surfaces.

A crack growth technique was developed from Reference 29. The loading on the specimen was 15 - 60 kN (2.2 - 8.7 Kip) for approximately 10,000 - 15,000 cycles at 5 Hertz. The crack initially grows on the inner surface but eventually breaks through the thickness to give a semi-circular crack front. As the crack grows further it becomes more like a simple "through-crack" with a similar crack length on both surfaces of approximately 40 mm.

This crack defect is similar in size and shape to that in the specimen supplied from the USAF F-111G wing.

Specimen patching

All areas of the specimen surface and fasteners that are bond surfaces are carefully solvent cleaned, grit blasted with aluminium oxide and treated with an adhesion promoter (Union Carbide A-187 silane coupling agent is brush applied continually for 15 minutes then oven dried at 80°C for one hour) to ensure a good bond surface. This treatment is the same as that carried out for the repair on RAAF aircraft A8-145.

Patches are made from Boron / Epoxy pre-preg fibre composite 5521-4 and are not as wide or long as the patch applied to RAAF aircraft A8-145. The patches are bonded to the specimens using FM-73 adhesive and cured under autoclave conditions (8 hours at 80°C). The repair cure cycle is an equivalent to that carried out on the aircraft. Ultrasonic 'A' scans or 'C' scans of the patched area are done to confirm patch and bond integrity.

Strain gauges

Two specimens were prepared with an array of strain gauges in the central area of the specimen at locations that matched some of those used on the full scale wing test. The first specimen (*FLTP27-4*) had them fitted as shown below in Figure 27.

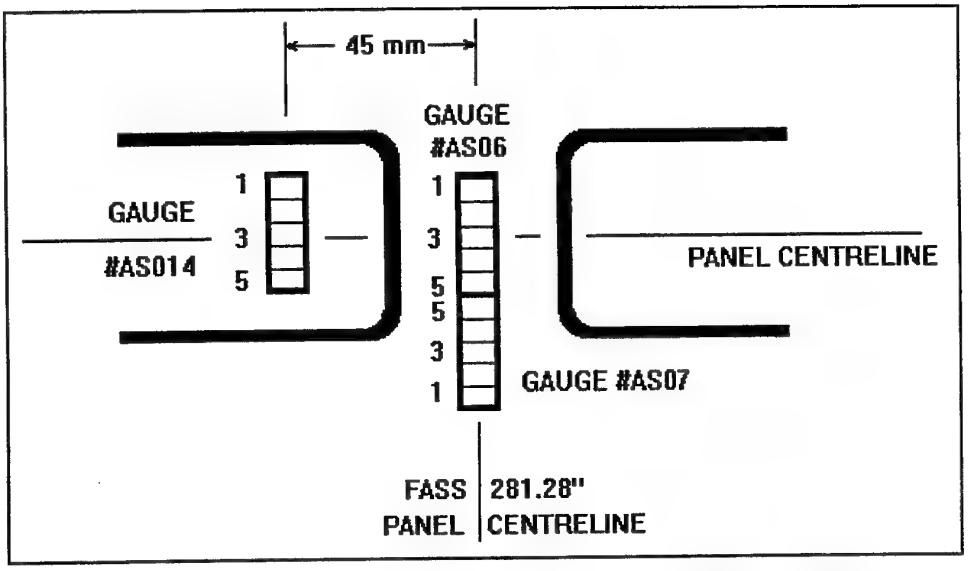

Figure 27. Details of strain gauge locations in central area of specimen FLTP27-4. *View down onto side representing upper surface of lower wing skin.*

Note that the gauges on the lower face #BS06 , #BS07 , #BS014 are aligned through the thickness so that they are opposite the ones on the upper face as follows :

Upper surface gauge #	AS06-1	AS06-2	AS06-3	AS06-4	AS06-5
Lower surface gauge #	BS06-1	BS06-2	BS06-3	BS06-4	BS06-5
Upper surface gauge #	AS07-1	AS07-2	AS07-3	AS07-4	AS07-5
Lower surface gauge #	BS07-1	BS07-2	BS07-3	BS07-4	BS07-5
Upper surface gauge #	AS014-1	AS014-2	AS014-3	AS014-4	AS014-5
Lower surface gauge #	BS014-1	BS014-2	BS014-3	BS014-4	BS014-5

Figure 28. Strain gauge identification numbering (FLTP27-4).

The second specimen (*FLTP27- 11*) also had fasteners installed to allow the fitment of the bending restraint as required; it was more extensively gauged were installed as shown below in Figure 29.

Thirty-seven channels of strain gauges were fitted to the specimen. Two channels were fitted to the bending restraint. Fifteen axial strain gauges were fitted to the side of the specimen representing the outer surface of the lower wing skin of the aircraft in positions. These replicated the gauges fitted to an aircraft wing in previous testing. Fifteen gauges were also fitted (in a mirror image) on the opposite surface of the specimen.

The strip type used was KYOWA KFG-1-120 019-23N10C2 with a gauge factor of 2.16.

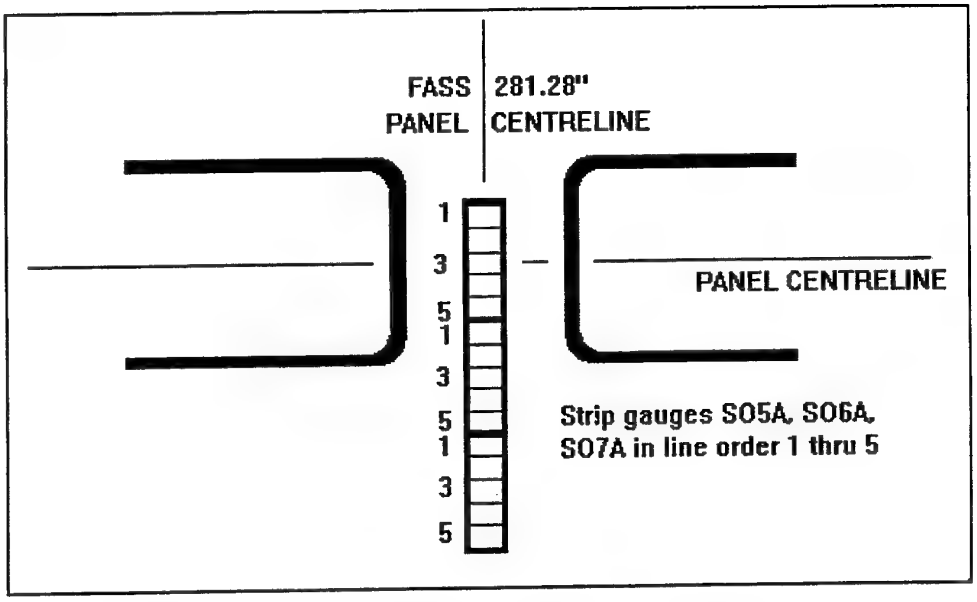

Figure 29. Strain gauge locations in central area of specimen FLTP27-11
View onto side representing upper surface of lower wing skin.

Note :

The gauges on the opposite side, representing the lower surface of the lower wing skin (SO5, S06, S07) are aligned through the thickness so that they are opposite their alike numbered gauge, as follows :

Upper surface gauge	S05A-1	S05A-2	S05A-3	S05A-4	S05A-5
Lower surface gauge	S05-1	S05-2	S05-3	S05-4	S05-5
Upper surface gauge	S06A-1	S06A-2	S06A-3	S06A-4	S06A-5
Lower surface gauge	S06-1	S06-2	S06-3	S06-4	S06-5
Upper surface gauge	S07A-1	S07A-2	S07A-3	S07A-4	S07A-5
Lower surface gauge	S07-1	S07-2	S07-3	S07-4	S07-5

Figure 30. Strain gauge identification numbering (FLTP27-11).

Also, six axial gauges and one rosette gauge were fitted to investigate far-field strains remote from the central area.

The axial type used was KYOWA KFG-5-350-C1-23 (Gauge Factor 2.18).

The rosette type used was TML (Gauge Factor 2.14).

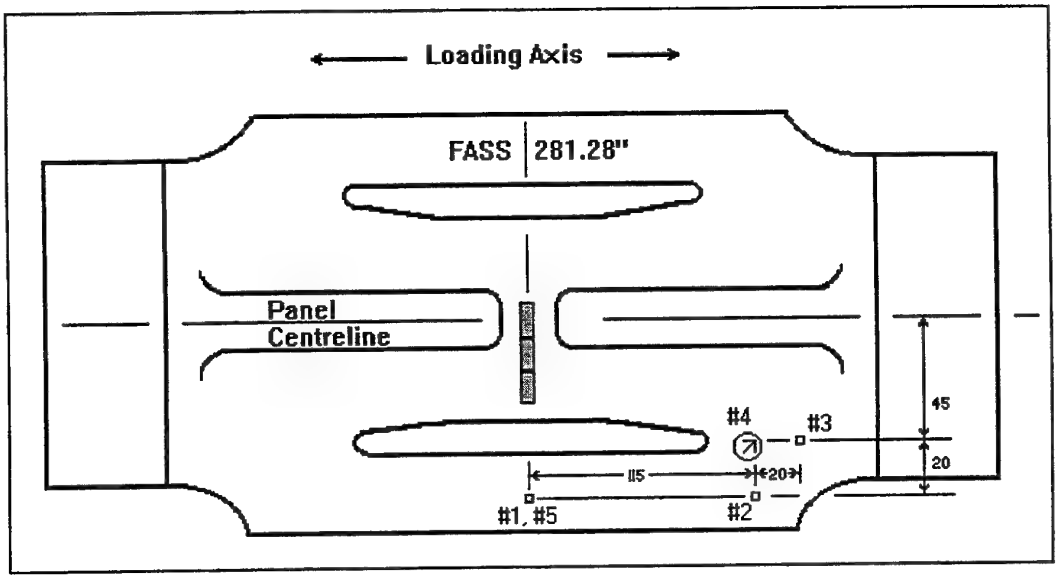

Figure 31. Strain gauge locations on specimen FLTP27-11
View on side representing upper surface of aircraft lower wing skin.

Note :

Rosette gauge is shown as circle , Strip gauges as rectangles and Axial gauges as squares. These gauges are all aligned with the load axis, except rosette gauge R-1 (perpendicular) and R-3 (at 45 degrees).

Gauges shown shaded are located on both sides of specimen.

Other gauges ,#2, #3, #4 are located only on side of specimen representing outer / lower surface of aircraft lower wing skin.

Two of the bending restraints were made (refer to Appendix 3) and for the test with *FLTP27-11,* one was strain gauged as shown below in Figure 32.

The axial type used was KYOWA KFG-5-350-C1-23 (Gauge Factor 2.18).

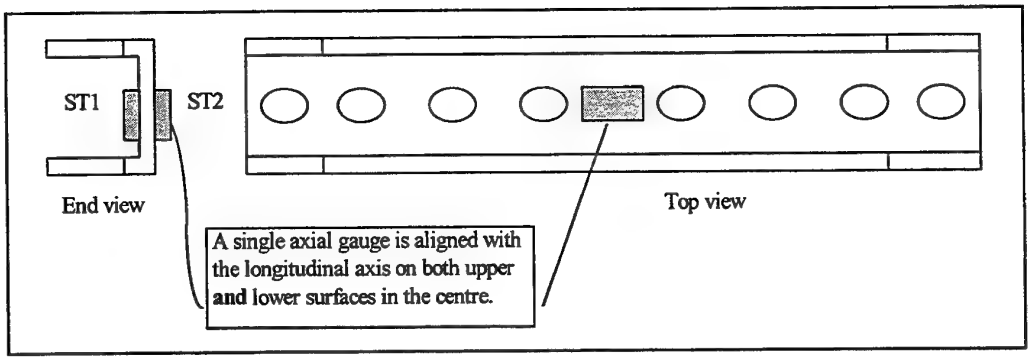

Figure 32. Strain gauge locations on bending restraint

THIS PAGE INTENTIONALLY BLANK

Appendix 3

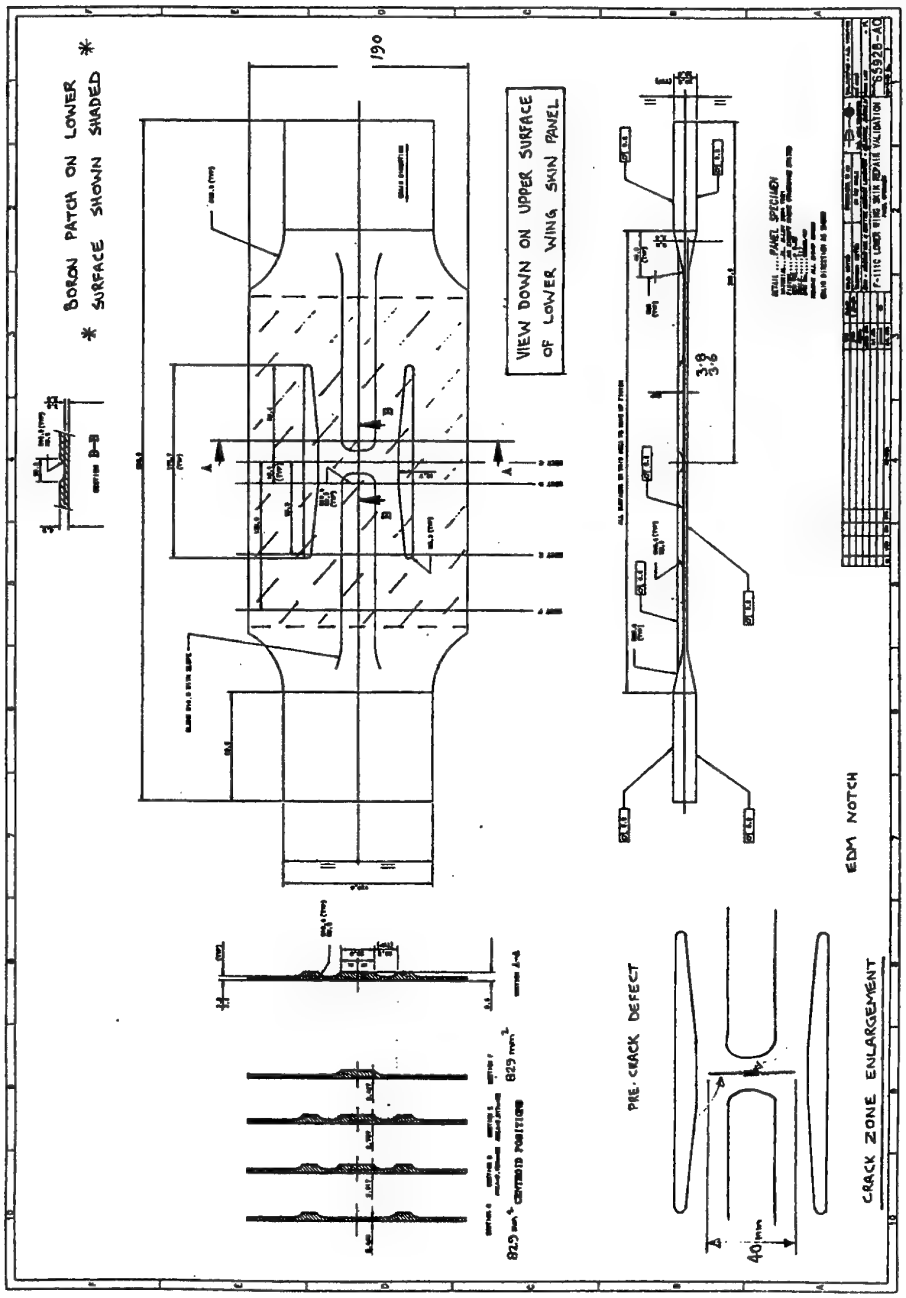

Figure 33. Panel specimen with boron patch repair

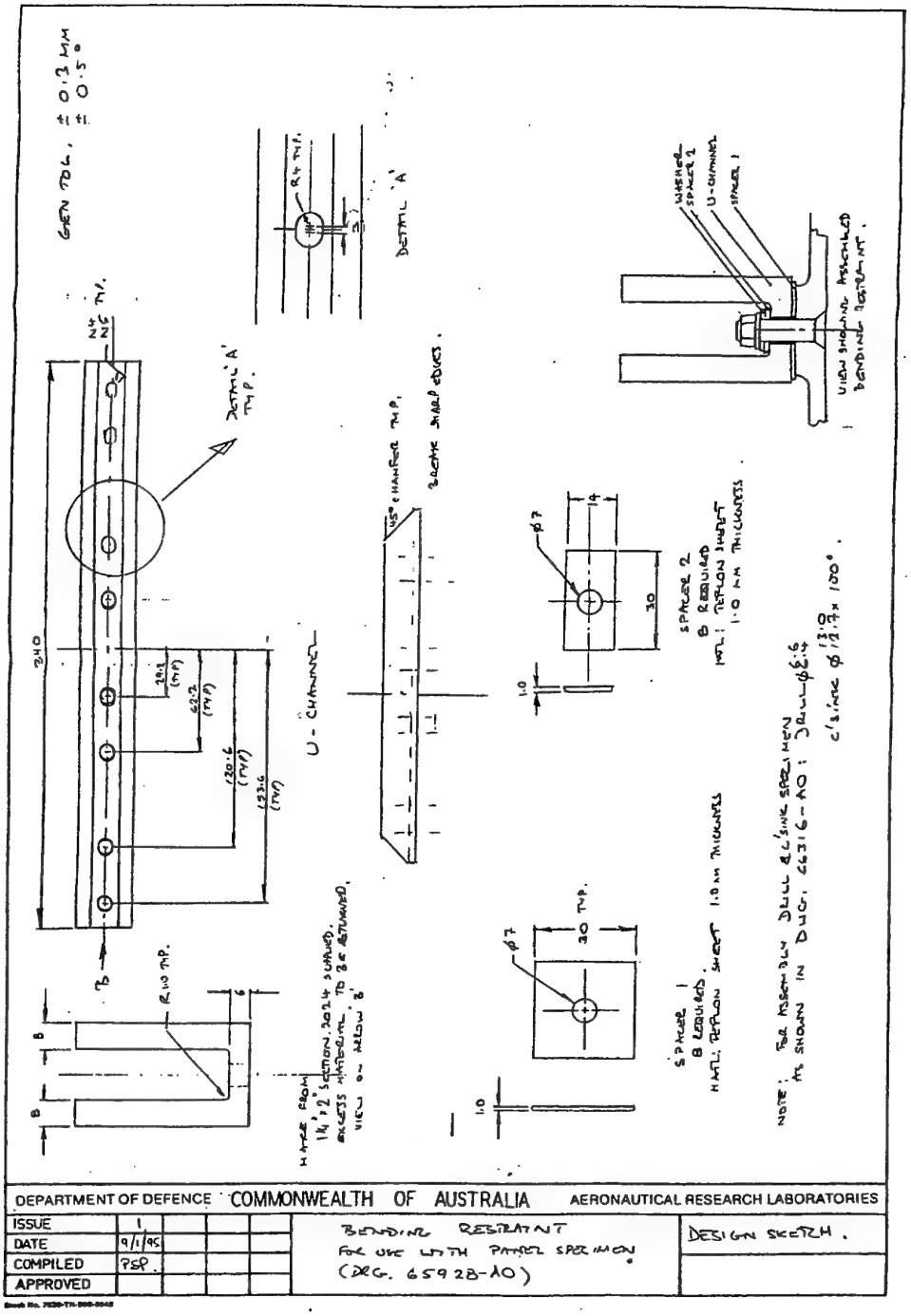

Figure 34. Bending restraint sketch

Appendix 4

First Box specimen

Specimen geometry

The specimen material is Aluminium 2024 - T851 and is machined to final size with no curvature, whereas the aircraft skin is machined, brake-formed to get a chordwise curvature, then chemical - milled to final size before assembling and shot-peening of the outer surface.

The box specimen is designed to incorporate the out-of-plane support provided by the wing spars and is large enough to install a full-size repair patch. The specimen test section is an assembly of two skins and three webs (representative of the Forward Spar, Forward Auxiliary Spar (FAS), and Centre spar). Each skin contains a test section that is a full-scale replica (other than skin curvature profile) of the fuel flow passage in the lower wing skin at FASS 281.28. The fastener spacing and nominal size is the same as the aircraft, however, the first specimen has clearance fit holes to ensure no shear load transfer between the skin and webs. The second specimen has interference fit fasteners along the middle web (FAS); the same as that used on the aircraft (0.25" csk Taper Lok bolts). A "tongue" adaptor, to mate with the grips of the testing machine, is attached each end so that loads can be applied to the specimen.

A view of one of the box specimen skins is shown below in Figure 35. An exploded view of the box specimen assembly is shown in Section 4.

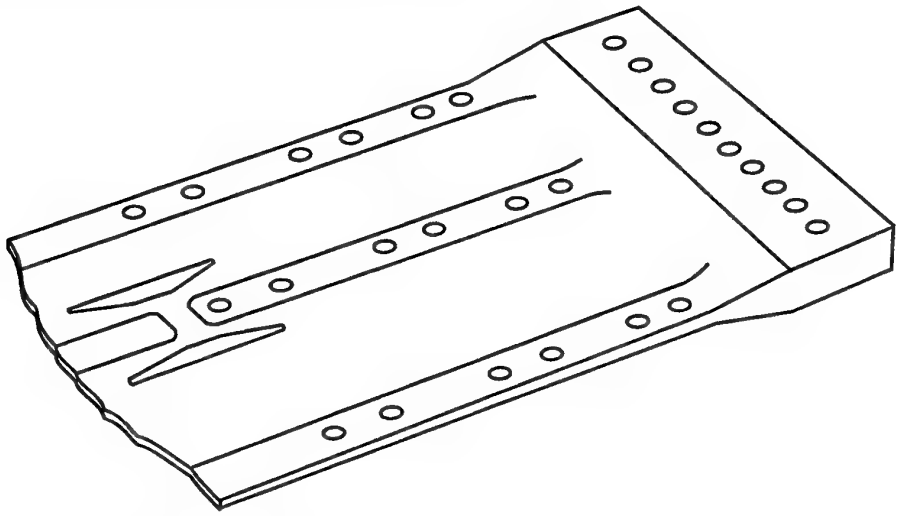

Figure 35. View onto box specimen skin showing inner surface

Specimen Preparation

The specimen is hand finished after manufacture by polishing out machining marks and scratches in the central test section with P1200 wet and dry paper.

Strain gauges were fitted to the first box specimen as described below.

Strain gauge locations (Stage 1)

Twenty-four channels of strain gauges were fitted to the specimen during the first stage of testing of just one skin with the three webs and tongue adaptors.

Ten axial strain gauges were fitted (as two strips of five) to the side of the specimen representing the outer surface of the lower wing skin of the aircraft. These gauge locations replicated those on a full size aircraft wing in previous testing.

The strip type used was KYOWA KFG-1-120 019-23N10C2

Two gauges were also fitted (in a mirror image of the centre gauge of each strip) on the opposite surface of the specimen.

The axial type used was KYOWA KFG-5-350-C1-23 (Gauge Factor 2.15).

Four rosette gauges were fitted ; three to the side representing the inner surface and one to the outer surface.

The rosette type used was TML (Gauge Factor 2.14).

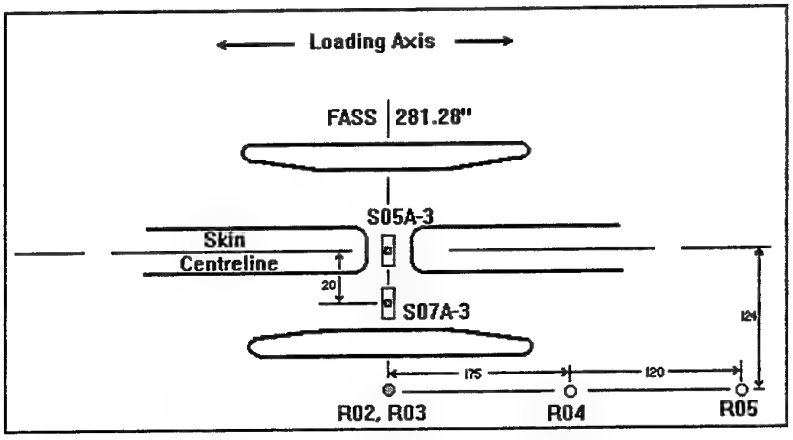

Figure 36. Strain gauge locations on Box 1, Skin 2.
View onto side representing inner surface of lower wing skin.

Note : Rosette gauges are shown as circles , Strip gauges as rectangles and Axial gauges as squares. These gauges are all aligned with the load axis, except the rosette gauge arm #1 (at +45 degrees towards the skin centreline) and rosette arm #2 (at -45 degrees ie away from the centreline).

Gauges shown shaded are located on both sides of specimen.

Other gauges ; R02, S05-1 thru -5, S07-1 thru -5 are located on the side of specimen representing the outer surface of aircraft lower wing skin.

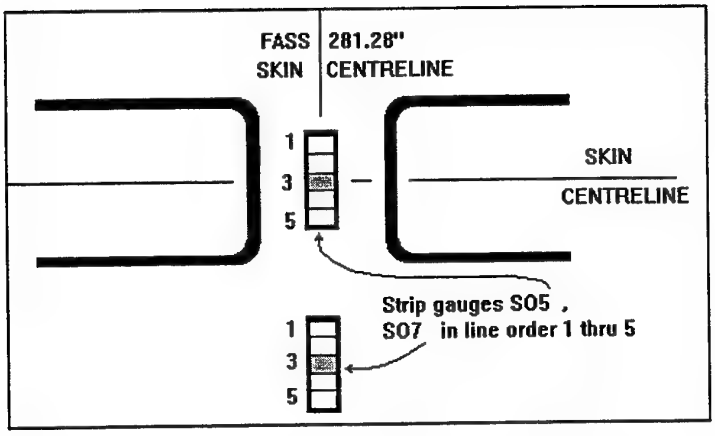

Figure 37. Details of strain gauge locations in central area of Box 1, Skin 2.

Note:

The gauges on the opposite side, representing the upper surface of the lower wing skin (SO5A-3, S07A-3 shown shaded) are aligned through the thickness so that they are opposite their alike numbered gauge, as follows :

Upper surface gauge			S05A-3		
Lower surface gauge	S05-1	S05-2	S05-3	S05-4	S05-5
Upper surface gauge			S07A-3		
Lower surface gauge	S07-1	S07-2	S07-3	S07-4	S07-5

Figure 38. Strain gauge identification (Box 1, Skin 2)

Specimen pre-cracking

This procedure requires the removal of thirteen strain gauges in the central area of the specimen. These are identified as RO2-1 thru -3, SO5A-3, SO7A-3, SO5-1 thru -5, SO7-1 thru -5.

The introduction of the crack defect into the specimen skins was achieved by creating a notch on the side of the specimen skin representing the upper surface of the lower wing skin. The notch (created by EDM) does not extend through to the other surface; it is a semi-circular slit approximately 0.1 mm wide and 35 mm long extending to a maximum depth of 3.5 mm.

The specimen is partially assembled with all three spars but only one skin and then loaded under cyclic tension loading until cracks appear at the each end of the notch and grow to the required length on both surfaces. The specimen is then disassembled and the procedure is repeated with the other skin. A crack growth technique was developed from previous testing and Reference 25. The tension loading on the specimen is cycled between 35 kN and 140 kN for approximately 71,000 to 74,000 cycles at 4 Hertz.

The crack initially grows on the inner surface but eventually breaks through the thickness to give a semi-circular crack front. As the crack grows further it becomes more like a simple "through crack" with a similar crack length on both surfaces of approximately 48 mm. This crack defect is similar in shape to that in the specimen supplied from the USAF F-111G wing. The different crack lengths used in the specimen types is due to the information received during the testing program. The initial estimate of the crack size in RAAF aircraft F-111C (A8-145) was 40 mm; for consistency, this value was used for all pre-cracked panel testing. A later measurement of the crack showed it to be 48 mm and this value was used for the later tests involving both box specimens.

Specimen patching

The repair patch is a 14 ply laminate made from Boron / Epoxy pre-preg fibre composite 5521-4, identical to that used on RAAF aircraft A8-145. The patch is bonded in place with FM-73 adhesive under heat blanket / vacuum bag conditions for eight hours at 80°C. A patch was applied to the external surface of both pre-cracked skins (representing the outer surface of the lower wing skin) on the specimen. Both patches were cured simultaneously.

Eleven strain gauges were then installed; five on each boron patch and one on the central spar inside the specimen, as described below.

Strain gauge locations (Stage 2)

Twenty-two channels of strain gauges were fitted to the specimen when completely assembled, with both skins pre-cracked and patched, for the second stage.

Five axial strain gauges were fitted over the boron patch on each of the skin panels.
The gauge type used was CEA-06-250UN-350 with a gauge factor of 2.10.

One axial strain gauge was located at the mid-point of the web of the central spar
The axial type used was KYOWA KFG-5-350-C1-23 (Gauge Factor 2.105).

Three rosette gauges R03, R04, R05 , installed for stage 1, were left fitted to the inside of *Box 1, Skin 2* .
These gauges are all aligned parallel with the load axis, except rosette gauge arms #1 (at +45 degrees) and #2 (at -45 degrees).

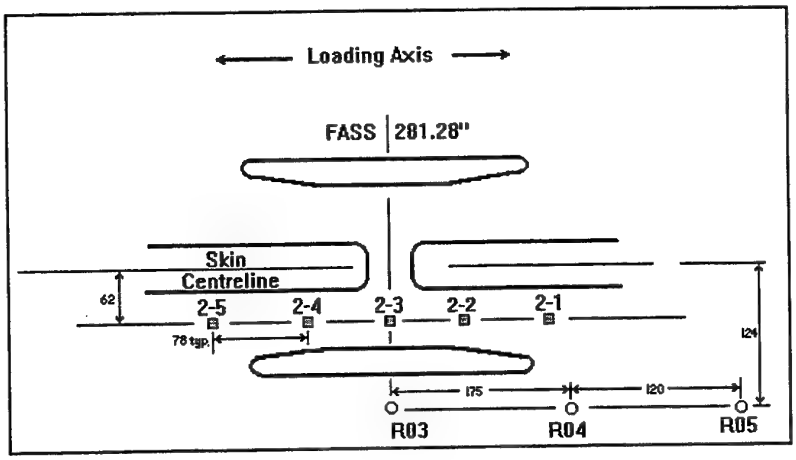

Figure 39. Strain gauge locations - View onto inner surface of Skin 2 *of fully assembled* Box 1 *specimen.*

Note : Rosette gauges are shown as circles and Axial gauges as squares.
Gauges shown shaded are located on outside of specimen.
Gauges R02, S05A-3, S07A-3, S05-1 thru -5, S07-1 thru -5 have been removed to allow pre-cracking and patch application.

Specimen painting

The specimen external surface was cleaned of grease and dirt after assembly and application of the boron repair patch and strain gauges was completed. A coating of low emissivity paint (RADIO SPARES stock no. 496-782 - Matt Black Radiator Paint) could be applied to assist thermal analysis of the test section.

Second Box Specimen

Specimen description

The second specimen was prepared and assembled as per the first specimen, with the following exceptions :

- The pre-cracking was done to one skin at a time; the three spars were connected but the centre web had undersize fasteners (3/16" diameter) to allow for special tapered holes in the final installation.
- The clearance-fit screw-type fasteners connecting the centre web to the skins were replaced with interference-fit Taper-Lok fasteners, as used at the same location on the F-111C aircraft wing skin. However, the countersinks in the skins were already machined for the larger heads of the first type of fastener. For those fasteners covered by the boron patch, the gap was filled flush to the surrounding skin surface with FM-73 adhesive during the patch bonding.

- The strain gauges were fitted to the skin and to one of the patches prior to the simultaneous bonding of both patches so that the residual strains induced by the cure cycle could be determined. Strain surveys were done before and after the specimen was fully assembled with both patches installed. This technique required the strain gauge wiring to be removed for the bonding process (to minimise uneven pressure on the patch during the bonding process) and refitted afterwards.

Strain surveys

The array of gauges shown below in Figure 40 were installed on to *Box 2, Skin 1* prior to the bonding of the patches to the skins. This array replicates most of the same locations on the panel specimens FLTP69-3 and FLTP69-4 and some of those on the full-scale wing test.

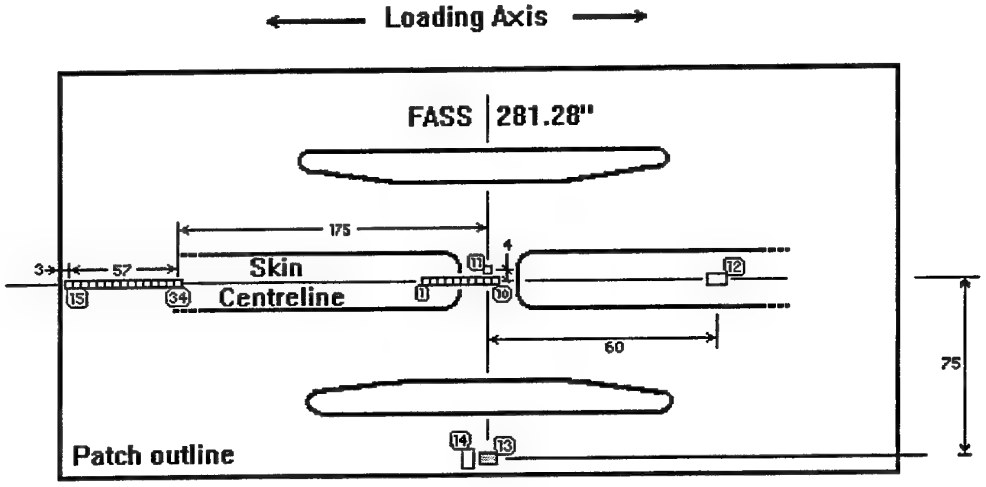

Figure 40. View onto Box 2, Skin 1 *specimen shows strain gauge locations on boron patch relative to skin geometry.*

Note that gauge #G10 is located on the side representing upper surface of lower wing skin (opposite gauge #13 shown shaded). Gauge #14 is the only gauge aligned perpendicular to the loading axis.

#1 - #10, #11 Kyowa KFG 120 D9 11N10C2 Gauge factor 2.10
#12- #14 Micro Measurements CEA-06 250 UN Gauge factor 2.10
#G10 Kyowa WK-13 125 BT Gauge factor 2.12
#15 - #34 Kyowa KFG 120 D19 11N10C2 Gauge factor 2.10

Strain surveys were taken at regular intervals during the fatigue cycling. Initial testing showed unexpected crack growth behaviour, and more strain gauges were fitted to the *Box 2* specimen to determine the far-field strain values.

To give a more detailed analysis, a further array of eight strain gauges were fitted to the specimen whilst mounted in situ in the testing machine with no applied loads. Because the maximum number of strain gauges that can be surveyed in one configuration is 38 (plus two channels for test machine load and displacement) with the current equipment, the gauges #15 thru #34 were omitted from sampling after one and a half blocks of cyclic loading had been applied to the specimen.

The new axial 350Ω gauges were numbered #36, 36B, 37, 38, 38B, 39, 40 , 41 and located on skin 1 as shown below. All gauges had a gauge factor of 2.10, except #38 and #37 which had 2.09.

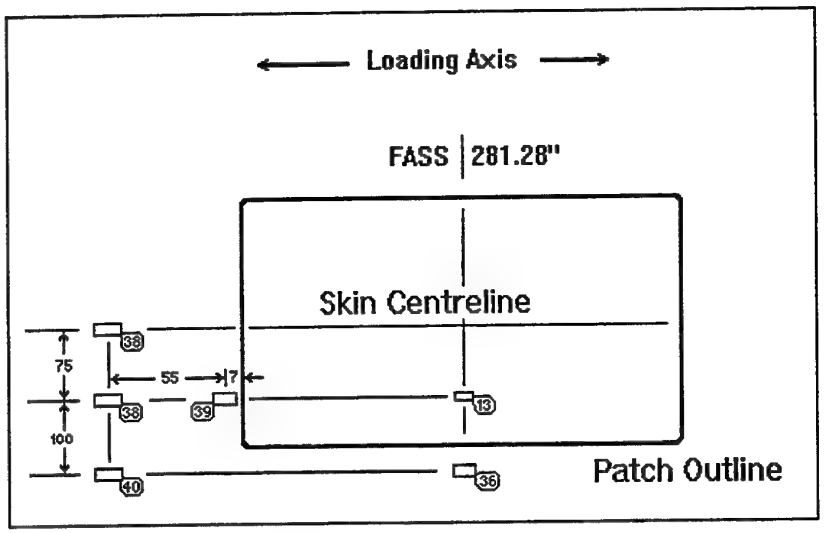

Figure 41. View onto second box specimen showing additional strain gauge locations (after patch cure) on Box 2, Skin 1.

Note that gauge #41 was fitted to the centre of the side spar, in line with FASS 281.28 adjacent to gauge #36. Gauges #36B and #38B were fitted to *Skin 2* , in the same locations as gauges #36 and #38, respectively, on *Skin 1*.

DISTRIBUTION LIST

F-111C Lower Wing Skin Bonded Composite Repair Substatiation Testing
R. Boykett and K. Walker

AUSTRALIA

DEFENCE ORGANISATION

Task Sponsor DTA

S&T Program

Chief Defence Scientist
FAS Science Policy
AS Science Industry and External Relations
AS Science Corporate Management
} shared copy

Counsellor Defence Science, London (Doc Data Sheet)
Counsellor Defence Science, Washington (Doc Data Sheet)
Scientific Adviser to MRDC Thailand (Doc Data Sheet)
Director General Scientific Advisers and Trials/Scientific Adviser Policy and Command (shared copy)
Navy Scientific Adviser (3 copies Doc Data Sheet and one copy of the distribution list)
Scientific Adviser - Army (Doc Data Sheet and distribution list only)
Air Force Scientific Adviser
Director Trials

Aeronautical and Maritime Research Laboratory
Director

Electronics and Surveillance Research Laboratory
Director

Chief of Airframes and Engines Division
Research Leader
R. Boykett
K. Walker

DSTO Library
Library Fishermens Bend
Library Maribyrnong
Library DSTOS (2 copies)
Australian Archives
Library, MOD, Pyrmont (Doc Data sheet only)

Forces Executive

Director General Force Development (Sea) (Doc Data Sheet only)
Director General Force Development (Land), (Doc Data Sheet only)
Director General Force Development (Air)

Army

ABCA Office, G-1-34, Russell Offices, Canberra (4 copies)

Air Force

Wing Commander E. Wilson, OIC ASI, HQLC, RAAF Williams, Laverton VIC
Flight Lieutenant S. White, SRLMSQN, RAAF Amberley, QLD
Mr M. Davis ATS1A, 501 Wing, RAAF Amberley, QLD

S&I Program

Defence Intelligence Organisation
Library, Defence Signals Directorate (Doc Data Sheet only)

B&M Program (libraries)

OIC TRS, Defence Central Library
Officer in Charge, Document Exchange Centre (DEC), 1 copy
*US Defence Technical Information Centre, 2 copies
*UK Defence Research Information Center, 2 copies
*Canada Defence Scientific Information Service, 1 copy
*NZ Defence Information Centre, 1 copy
National Library of Australia, 1 copy

UNIVERSITIES AND COLLEGES

Australian Defence Force Academy
Library
Head of Aerospace and Mechanical Engineering
Deakin University, Serials Section (M list), Deakin University Library, Geelong, 3217
Senior Librarian, Hargrave Library, Monash University
Librarian, Flinders University

OTHER ORGANISATIONS

NASA (Canberra)
AGPS

OUTSIDE AUSTRALIA

ABSTRACTING AND INFORMATION ORGANISATIONS

INSPEC: Acquisitions Section Institution of Electrical Engineers
Library, Chemical Abstracts Reference Service
Engineering Societies Library, US
Materials Information, Cambridge Scientific Abstracts, US
Documents Librarian, The Center for Research Libraries, US

DEFENCE SCIENCE AND TECHNOLOGY ORGANISATION
DOCUMENT CONTROL DATA

1. PRIVACY MARKING/CAVEAT (OF DOCUMENT)

2. TITLE

F-111C Lower Wing Skin Bonded Composite Repair Substatiation Testing

3. SECURITY CLASSIFICATION (FOR UNCLASSIFIED REPORTS THAT ARE LIMITED RELEASE USE (L) NEXT TO DOCUMENT CLASSIFICATION)

Document	(U)
Title	(U)
Abstract	(U)

4. AUTHOR(S)

R. Boykett and K. Walker

5. CORPORATE AUTHOR

Aeronautical and Maritime Research Laboratory
PO Box 4331
Melbourne Vic 3001

6a. DSTO NUMBER	6b. AR NUMBER	6c. TYPE OF REPORT	7. DOCUMENT DATE
DSTO-TR-0480	AR-010-110	Technical Report	November 1996

8. FILE NUMBER	9. TASK NUMBER	10. TASK SPONSOR	11. NO. OF PAGES	12. NO. OF REFERENCES
M1/8/1027	AIR 94/118	DTA	67	36

13. DOWNGRADING/DELIMITING INSTRUCTIONS

None

14. RELEASE AUTHORITY

Chief, Airframes and Engines Division

15. SECONDARY RELEASE STATEMENT OF THIS DOCUMENT

Approved for public release

OVERSEAS ENQUIRIES OUTSIDE STATED LIMITATIONS SHOULD BE REFERRED THROUGH DOCUMENT EXCHANGE CENTRE, DIS NETWORK OFFICE, DEPT OF DEFENCE, CAMPBELL PARK OFFICES, CANBERRA ACT 2600

16. DELIBERATE ANNOUNCEMENT

No Limitations

17. CASUAL ANNOUNCEMENT Yes

18. DEFTEST DESCRIPTORS

Cyclic loads, fatigue test, fiber laminates, repair, F-111 aircraft

19. ABSTRACT

Experimental testing was undertaken to verify a bonded composite repair to a crack in the primary structure of a F-111C aircraft of the Royal Australian Air Force. The flight safety was compromised by a crack in the lower wing skin reducing the structure residual strength below the Design Limit level. Two levels of representative specimens were designed to incorporate the complex local geometry in the lower wing skin. They were tested in several configurations (ambient, high and low temperature) under static and cyclic loads with, and without, repaired cracks. Extensive strain survey data was obtained for both types of specimens and their static residual strength was shown to be restored by the repair. Cyclic loading tests of specimens with the repair also demonstrated good durability and damage tolerance, with crack growth data providing a recommended inspection interval for remaining aircraft.

INFORMATION EXCHANGE AGREEMENT PARTNERS

Acquisitions Unit, Science Reference and Information Service, UK
Library - Exchange Desk, National Institute of Standards and Technology, US

SPARES (10 copies)

Total number of copies: 58